

**Systematic Analysis of K-feldspar $^{40}\text{Ar}/^{39}\text{Ar}$ Step Heating Results II:
Relevance of Laboratory Argon Diffusion Properties to Nature**

OSCAR M. LOVERA¹, MARTY GROVE¹, AND T. MARK HARRISON^{1,2}

¹*DEPARTMENT OF EARTH & SPACE SCIENCES AND IGPP
UNIVERSITY OF CALIFORNIA, LOS ANGELES, LOS ANGELES, CA 90095-1567, USA*

²*RESEARCH SCHOOL OF EARTH SCIENCES
THE AUSTRALIAN NATIONAL UNIVERSITY, CANBERRA, A.C.T. 0200, AUSTRALIA*

Abstract – We examine a database containing the results of $^{40}\text{Ar}/^{39}\text{Ar}$ step-heating experiments performed on 194 basement K-feldspars to recover thermal history information. Qualitative examination of $^{40}\text{Ar}/^{39}\text{Ar}$ systematics reveals that about half of the K-feldspars examined are sufficiently well-behaved to be suitable for thermal history analysis. Correlation algorithms are developed to quantitatively assess the degree to which age and ^{39}Ar release spectra are compatible with the same volume diffusion process. Upon applying these methods, we find that 65% of all samples yield correlation coefficients in excess of 0.8 while roughly 40% give values above 0.9. We further compare the observed correlation behavior with that predicted from the multi-diffusion domain (MDD) model and find good agreement for samples with correlation coefficients above 0.9. In contrast, hydrous phases unstable under *in vacuo* heating and K-feldspars with highly disturbed age spectra yield poorly correlated age and diffusion properties. The high degree of correlation exhibited by the majority of K-feldspars we have analyzed validates extrapolation of experimentally determined diffusion properties to conditions attending natural Ar loss within the crust. Despite this, a significant number of basement K-feldspars analyzed by the step-heating method yield $^{40}\text{Ar}/^{39}\text{Ar}$ systematics that are clearly problematic for thermal history analysis. We numerically explore the effects of low-temperature alteration of K-feldspar upon thermochronological analysis and identify a range of conditions under which information is progressively lost. Finally, we demonstrate the insensitivity of thermal history calculations to detailed knowledge of the diffusion mechanism by introducing the heterogeneous diffusion (HD) model. We find that the MDD approach can successfully recover imposed thermal histories from HD-type crystals and conclude that most details of the interpretive model employed are of secondary importance. The only requirement for recovering thermal histories from K-feldspar $^{40}\text{Ar}/^{39}\text{Ar}$ step-heating results is that argon loss proceeds by volume diffusion and that laboratory argon release adequately mimics the natural diffusion boundaries and mechanisms – a requirement implicitly met by those samples exhibiting high degrees of correlation.

1. INTRODUCTION

Because tectonic processes characteristically alter the distribution of heat within the crust, the ability to determine time-dependent paleotemperature variations using mineral thermochronometry has increasingly been viewed as fundamental data for deciphering the evolution of basement rocks. Thermochronometry via the $^{40}\text{Ar}/^{39}\text{Ar}$ method involves modeling of the inhomogeneous internal distributions of radiogenic ^{40}Ar ($^{40}\text{Ar}^*$) produced by diffusion in silicate minerals (MCDUGALL and HARRISON, 1999). Such modeling invariably requires experimental calibration of mineral diffusion properties before quantitative thermal history estimates can be produced. Because these calibrations are necessarily performed at higher temperatures and shorter time scales than those relevant to diffusion in nature, the most fundamental issue in thermochronometry is the relevance of laboratory-determined diffusion properties to argon transport within minerals under crustal conditions.

The most promising opportunity to test this fundamental assumption is provided by step-heating experiments performed with K-feldspar. Currently, there are essentially three ways to gather relevant information about argon diffusion in silicate minerals. These include incremental extraction of ^{40}Ar from a bulk sample in $^{40}\text{Ar}/^{39}\text{Ar}$ step-heating experiments (BERGER and YORK, 1981), direct mapping of $^{40}\text{Ar}/^{39}\text{Ar}$ gradients via laser ablation from an array of regularly spaced melt pits (ONSTOTT et al., 1991), and laser depth profiling (ARNAUD and KELLEY, 1997). Laser spot mapping permits ca. 20 μm scale imaging of isotope distributions along grain surfaces, but does not permit study of smaller features that may serve as important diffusion boundaries. While laser depth profiling (KELLEY et al., 1994) can improve the spatial resolution in the near-surface region by 2 orders of magnitude (i.e., 0.1 μm), analysis of potential diffusion boundaries is limited to original grain boundaries, cleavages, and similar features of large lateral extent exposed at the surface of grains. Step-heating methods therefore represent the only approach capable of providing volume information from the material. Although isotope distributions are not directly imaged, the natural loss mechanism is potentially reproduced.

Alkali feldspar is the most prevalent potassium-rich silicate of wide crustal occurrence that is sufficiently stable during *in vacuo* heating to provide a reasonable expectation that natural $^{40}\text{Ar}^*$ diffusion properties could be reproduced in laboratory step-heating experiments (MCDOUGALL and HARRISON, 1999). While isothermal, hydrothermal treatment of hydrous phases is possible, our ability to interpret such experiments is limited to bulk fusion and laser spot analysis. Moreover, the database of argon diffusion measurements in hydrous phases is relatively small (BALDWIN et al., 1990; FOLAND, 1974; GILETTI, 1974; GROVE and HARRISON, 1996; HARRISON et al., 1985; HARRISON and MCDOUGALL, 1981). In contrast, many hundreds of diffusion experiments have been performed with K-feldspars sampled from a wide range of geologic environments (LOVERA et al., 1997). The microstructural and overall stability of K-feldspar to 1100°C during *in vacuo* step-heating has been well documented (see, LOVERA et al., 1993).

The multi-diffusion domain (MDD) model has proven capable of describing the full range of laboratory argon diffusion behavior exhibited by basement K-feldspars (LOVERA et al., 1997). The leading alternative, the multi-path model (LEE, 1995), can only approximate the observed diffusion behavior when its fundamental characteristic (i.e., interaction between diffusion domains) is minimized to such an extent that it becomes indistinguishable from the MDD approach (ARNAUD and KELLEY, 1997). The MDD model represents argon transport in K-feldspars as being controlled by volume diffusion processes acting upon a distribution of length scales. It has been extensively tested and developed in the more than one decade since its inception (HARRISON et al., 1993; HARRISON et al., 1994; LOVERA et al., 1997; LOVERA et al., 1993; LOVERA et al., 1989; LOVERA et al., 1991; QUIDELLEUR et al., 1997; RICHTER et al., 1991). While the ability of the MDD model to represent laboratory diffusion properties has become firmly established, its ability to successfully recover basement thermal histories has been repeatedly questioned and remains controversial (ARNAUD and KELLEY, 1997; BURGESS et al., 1992; FOLAND, 1994; PARSONS et al., 1999; PARSONS et al., 1988).

Our principal goals in this paper are to: (1) identify problematic behavior in K-feldspar $^{40}\text{Ar}/^{39}\text{Ar}$ age spectra for thermal history recovery; (2) examine our database of K-feldspar step-heating experiments to determine the frequency with which misbehaving samples occur; and (3) quantitatively evaluate the compatibility of $^{40}\text{Ar}/^{39}\text{Ar}$ age and laboratory diffusion data from samples within this database to further determine the proportion of basement K-feldspar samples that are likely to be amenable to thermal history analysis. In discussing recent criticisms of the MDD model we also illustrate, by way of numerical simulation, how low-temperature recrystallization or an error in our assumption of the diffusion mechanism might impact calculated thermal histories. Combined with the results from our database samples, these calculations demonstrate the viability of recovering crustal thermal histories through application of the MDD model provided that appropriate samples are analyzed.

2. AN EXPANDED DATABASE OF K-FELDSPAR $^{40}\text{AR}/^{39}\text{AR}$ STEP-HEATING RESULTS

In this section, we systematically examine results from K-feldspars analyzed at UCLA from 1994 to 2000 (Table 1). This database is expanded over that presented in (LOVERA et al., 1997). The previous paper focused primarily upon the laboratory argon diffusion properties of K-feldspar and the ability of the MDD model to represent them. Our primary goal in the present paper is to evaluate the self-consistency of natural and laboratory argon diffusion in K-feldspar.

Simple volume diffusion theory predicts that age spectra should increase monotonically with progressive ^{39}Ar release because natural $^{40}\text{Ar}^*$ concentrations would be higher in more retentive sites (Fig. 1a). Exhibition of this predicted behavior must represent the initial criterion for selecting samples for thermal history analysis. In the discussion below, we recognize two principle types of misbehavior in which this criterion is violated: (1) contamination with excess radiogenic ^{40}Ar ($^{40}\text{Ar}_E$) and (2) development of maxima in the age spectrum that occur at intermediate stages of ^{39}Ar release. We first provide examples of these phenomena and then analyze the samples listed in Table 1 to determine the frequency at which basement K-feldspars with problematic characteristics are encountered in thermal history studies.

2.1 $^{40}\text{Ar}_E$ Contamination

Contamination of samples with $^{40}\text{Ar}_E$ has long been recognized as a serious problem in interpreting argon isotopic age results (MCDUGALL and HARRISON, 1999). Affected basement K-feldspars characteristically exhibit “U-shaped” patterns (Fig. 1b) with large quantities liberated at low-temperature (generally below $\sim 700^\circ\text{C}$) and again at high-temperature (typically above $\sim 1000^\circ\text{C}$) (HARRISON, 1990; ZEITLER and FITZGERALD, 1986). Generally, only ages yielded by the portion of the age spectrum corresponding to intermediate temperature release are consistent with independent geologic and geochronologic constraints (ZEITLER and FITZGERALD, 1986). Because release of $^{40}\text{Ar}_E$ at low temperature ($<700^\circ\text{C}$) tends to be correlated with Cl-derived ^{38}Ar , metamorphic fluids from decrepitating fluid inclusions are implicated as the source (HARRISON et al., 1993). In favorable instances, measured age spectra can be corrected for fluid inclusion derived $^{40}\text{Ar}_E$ (HARRISON et al., 1994). Unfortunately, while it is in many instances possible to clearly identify the effects of high-temperature $^{40}\text{Ar}_E$ (FOSTER et al., 1990), release of $^{40}\text{Ar}_E$ under these conditions is so unpredictable that reliable correction schemes have not been, and may never be, developed. Hence, the value of samples affected by high-temperature $^{40}\text{Ar}_E$ contamination (see, REDDY et al., 1999; VILLA, 1994; VILLA, 1990) for thermochronology is extremely limited and there is little point in considering them further within the context of the MDD model.

2.2 Intermediate Age Maxima

A second type of anomalous behavior is a maximum in the age spectrum that occurs at intermediate stages of ^{39}Ar release (Fig. 1c). Intermediate age maxima differ from features produced by $^{40}\text{Ar}_E$ contamination in two important respects. First they are typically developed over the interval of ^{39}Ar release that is least affected by $^{40}\text{Ar}_E$ contamination (compare Fig. 1b and 1c). Second, the ages of successive steps that define these maxima vary in a far more regular manner than is generally the case for samples heavily contaminated with $^{40}\text{Ar}_E$. Such smooth variation implies diffusive release of argon and leads us to conclude that the features are not another manifestation of excess $^{40}\text{Ar}_E$.

Age maxima such as those described above are characteristically exhibited by feldspars that have been partially to completely altered to adularia (FOLAND, 1994; GIRARD and ONSTOTT, 1991; WARNOCK and VAN DE KAMP, 1999). This association suggests that age maxima are produced by low-temperature processes since growth of sanidine structure K-feldspar (adularia) upon detrital K-feldspar is prevalent in diagenetic settings (KASTNER and SIEVER, 1979). Even K-feldspars derived from basement rocks may be altered to adularia. For example, basement K-feldspars immediately adjacent to basin unconformities or within mineralized zones affected by high fluid flow have been described as having been extensively replaced by low-temperature sanidine (MENSING, 1983). Intermediate age maxima may also result from low-temperature deformation. We have also found that intermediate age maxima tend to be yielded by K-feldspars that have been deformed in shallow, high-strain environments adjacent to brittle faults. The majority of samples affected by intermediate age maxima in Table 1 were collected from such settings. Clearly defined intermediate age maxima are not always associated with deformed K-feldspars, however (ARNAUD and EIDE, 2000; REDDY et al., 1999).

2.3 Survey of the Database for Problematic Behavior

In Table 1, we represent the frequency with which the above-mentioned misbehavior occurs among the K-feldspar $^{40}\text{Ar}/^{39}\text{Ar}$ age spectra. As indicated in Fig. 2a, roughly one third of the K-feldspar age spectra listed in Table 1 exhibit either intermediate age maxima (23%) or high-temperature $^{40}\text{Ar}_E$ (7%). In identifying K-feldspars that are contaminated by high-temperature $^{40}\text{Ar}_E$, we have included samples which vary erratically in age at high-temperature (Fig. 1b) and/or yield $^{40}\text{Ar}/^{39}\text{Ar}$ ages that are geologically unreasonable ages based upon independent constraints (FOSTER et al., 1990; HARRISON, 1990). Because it is not straightforward to detect samples only moderately affected by high-temperature $^{40}\text{Ar}_E$ contamination, it is likely that additional problematic samples in Table 1 have escaped our notice. In recognizing intermediate age maxima, we have restricted our focus to the portion of K-feldspar age spectra that is least affected by low- and/or high-temperature $^{40}\text{Ar}_E$ (typically 15-40% cumulative % ^{39}Ar

released; see Fig. 1b). Samples listed as exhibiting intermediate age maxima in Table 1 generally have the feature developed within this range of gas release.

Contamination of K-feldspar age spectra by low-temperature $^{40}\text{Ar}_E$ is an even more pervasive phenomena (Fig. 2b) which affects nearly all the samples in Table 1. However, because $^{40}\text{Ar}_E$ released at low-temperature appears to originate primarily from decrepitating fluid inclusions (HARRISON et al., 1993), it tends to be rapidly exhausted during progressive outgassing. Moreover, correction of the age spectrum for the effects of low-temperature $^{40}\text{Ar}_E$ contamination is often possible when age variation is correlated with release of Cl-derived ^{38}Ar (HARRISON et al., 1994). Because it is normally possible to reliably determine the portion of the age spectrum affected by low-temperature $^{40}\text{Ar}_E$ contamination when appropriate heating schedules are applied (i.e., isothermal duplicates), the primary issue regarding the quality of the age spectrum is how much of the measured age spectrum remains available for interpretation. When contamination is limited to only a few percent of ^{39}Ar release, ignoring the affected portion of the age spectrum does not represent a serious loss of information since about 75% of ^{39}Ar release from basement K-feldspar takes place below melting when high-resolution heating schedules are applied (Fig. 2c). For example, neglecting the low-temperature portion of the age spectrum that is contaminated with $^{40}\text{Ar}_E$ generally leaves about 66% of the ^{39}Ar release for modeling (Fig. 2d). However, the usable portion of the age spectrum tends to be substantially diminished for samples in Table 1 that have low-temperature $^{40}\text{Ar}_E$ in excess of 10% (Table 1; Fig. 2d). It is important to keep in mind that the age spectra of such heavily contaminated samples can often be corrected (HARRISON et al., 1994), significantly increasing the fraction of the age spectrum available for modeling.

Based upon results discussed above, we consider that about half of the K-feldspars in Table 1 yield $^{40}\text{Ar}/^{39}\text{Ar}$ systematics that are sufficiently “well behaved” samples in that they meet our initial criteria to attempt thermal history analysis using the MDD model. We wish to emphasize that the misbehavior is not randomly manifested. When it is discovered in one sample, we have found that there is a high

probability that nearby samples that have experienced the same geologic history will be similarly affected.

3. CORRELATION BETWEEN AGE AND LABORATORY DIFFUSION SPECTRA

The preceding qualitative analysis of our database of step-heating results from basement K-feldspars provides only a general impression of the frequency which samples yield age spectra compatible with simple volume diffusion theory. We now seek to take our analysis of database samples a step further. Under conditions of monotonic cooling, the MDD model predicts a high degree of correlation between the age spectrum (which typically represents millions to 100's of millions of years of $^{40}\text{Ar}^*$ accumulation) and the Arrhenius properties (which represents laboratory outgassing of reactor-derived ^{39}Ar over minutes to days). In order to express both functions with a common independent variable (cumulative ^{39}Ar released), we make use of the $\log(r/r_0)$ plot (RICHTER et al., 1991). This plot is constructed from the difference between measured $\log(D/r^2)$ values and those predicted by least square fitting of the characteristically linear array of initial, low-temperature $\log(D/r^2)$ data.

3.1. Quantifying Correlation between Age and $\log(r/r_0)$ Spectra

In the past we have qualitatively referred to correlated inflections in these spectra as strong evidence that laboratory ^{39}Ar diffusion in K-feldspar adequately mimics natural $^{40}\text{Ar}^*$ transport (LOVERA et al., 1993). In this section we present a quantitative approach for establishing the self-consistency of $^{40}\text{Ar}/^{39}\text{Ar}$ age and diffusion data. To quantify the compatibility of laboratory and natural argon transport properties as imaged by age and $\log(r/r_0)$ data, we have developed a method to calculate the cross-correlation between these spectra. Cross-correlation yields a measure of the similarity between discrete or continuous functions and is used extensively in many areas of science and engineering. For example, in geophysical applications it is used to determine the time shift needed to adjust seismic traces (TELFORD et al., 1990) or to measure the change and variance in waveform versus time and offset

(FRANKEL and CLAYTON, 1986). Cross correlation of two functions (f and g) $\{a,b\}$ is defined

as $\int_a^b f(x) \cdot g(x) dx$, or after normalization,

$$C_{fg} = \frac{\int_a^b f(x) \cdot g(x) dx}{\sqrt{\int_a^b f^2(x) dx \int_a^b g^2(x) dx}} \quad (1)$$

Note that the Cauchy-Buniakowsky-Schwarz integral inequality:

$$\int_a^b f^2(x) dx \int_a^b g^2(x) dx \geq \left[\int_a^b f(x) \cdot g(x) dx \right]^2 \quad (2)$$

ensures that C_{fg} is ≤ 1 . The C_{fg} value provides a measure of the similarity in shape of the two functions.

To simplify comparison between samples that exhibit a large spread of age and/or $\log(r/r_o)$ values we define f and g in the following manner:

$$f(x) = \text{age}(x) - \text{age}_i, \quad \text{age}_i = \frac{\int_a^b \text{age}(x) dx}{b-a} \quad (3)$$

$$g(x) = \log\left(\frac{r}{r_o}\right)(x) - \log_i, \quad \log_i = \frac{\int_a^b \log\left(\frac{r}{r_o}\right)(x) dx}{b-a} \quad (4)$$

These functions are further interpolated using a Chebyshev polynomial expansion or using a cubic spline interpolation (PRESS et al., 1988) to produce a discrete series of evenly spaced intervals. The series are then cross-correlated using the Fast Fourier Transform method (PRESS et al., 1988).

3.2. Application to $^{40}\text{Ar}/^{39}\text{Ar}$ Step-heating Data

In applying the method outlined in the previous section to K-feldspar $^{40}\text{Ar}/^{39}\text{Ar}$ step-heating data, we must define the integration limits (a,b) in equations (1)-(4). The lower limit (a) was established at the value of cumulative % ^{39}Ar release that corresponded to the point where release of low-temperature $^{40}\text{Ar}_E$ was no longer detectable. The upper limit (b) was set at the value of cumulative % ^{39}Ar release corresponding to the onset of melting (i.e., above 1100°C). Even when the interval of correlation could be extended by correcting for Cl-correlated $^{40}\text{Ar}_E$ (HARRISON et al., 1994), this was not done to ensure

that all samples were treated equally. In an effort to minimize the amount of interpretation at this stage of the calculations, we calculated the $\log(r/r_o)$ spectra of each of the samples using the average activation energy (46 kcal/mol) and frequency factor (10^5 s^{-1}) determined by (LOVERA et al., 1997) for a subset of these samples. In subsequent calculations requiring higher resolution, we determined the diffusion parameters of individual samples to calculate $\log(r/r_o)$ spectra.

Before presenting our results from all database samples, we believe it is helpful to identify relationships which greatly influence the value of C_{fg} obtained from equations (3) and (4). We have found that the value of C_{fg} primarily informs us of the similarity of the low-frequency properties of the age and $\log(r/r_o)$ spectra. Hence the sympathetic behavior (i.e., curvature and inflection points) of the age and $\log(r/r_o)$ spectra is of key importance.

In the following discussion, it is useful to focus upon the location of the crossover points where $f(x)$ and $g(x)$ are equal to their average values (x_f , x_g respectively). When x_f and x_g do not occur at the same value of cumulative % ^{39}Ar released, C_{fg} will be reduced because the integral $\int f \cdot g$ in (1) is negative in the $\{x_f, x_g\}$ interval. When the two spectra have similar curvature and increase monotonically (Fig. 3a and 3b), their crossover points tend to occur at the same value of cumulative % ^{39}Ar released and high values of C_{fg} are generally obtained. When the age and $\log(r/r_o)$ spectra both increase monotonically but have different curvature (Fig. 3c and 3d), the crossover points x_f and x_g diverge and the value of C_{fg} is decreased. Large reductions in C_{fg} can occur for samples with non-monotonic age spectra (see Fig. 3e and 3f). In fact, samples with intermediate age maxima account for the majority of the low C_{fg} values in Table 1. To summarize, only samples with monotonically increasing age and $\log(r/r_o)$ spectra of similar curvature yield C_{fg} values that closely approach unity (i.e. >0.90).

It is also informative to cross correlate age and $\log(r/r_o)$ spectra of materials in which the natural and laboratory argon transport properties are known to differ significantly. For example, 8-1-22 phengite, (Fig. 3g) yield a low $C_{fg} = 0.76$, while the 78-618 hornblende give a negative value of -0.78 . The low correlation here reflects progressively dissimilar modes of argon release in the laboratory and nature.

Laboratory Ar loss from the phengite is from the metastable dioctahedral dehydroxylate phase that is only moderately dissimilar from its natural precursor (GROVE and BEBOUT, 1995) whereas hornblende breaks down by incongruent melting (LEE et al., 1991). We infer that poorly-correlated K-feldspars (i.e., $C_{fg} < 0.8$) that are not heavily contaminated with $^{40}\text{Ar}_E$ probably possess laboratory diffusion properties that differ significantly from those which governed argon release in nature. Conversely, it follows that samples with $C_{fg} > 0.9$ have experienced only negligible changes in argon diffusion properties following ^{40}Ar closure in nature.

3.3. Analysis of Database Samples

Results obtained by cross-correlating the age and $\log(r/r_o)$ spectra of 194 K-feldspars are presented in Table 1 and illustrated in Fig. 4. As shown, 65% of all samples yield C_{fg} values in excess of 0.8 while roughly 40% of the samples give values above 0.9. The proportion of "well-behaved" samples indicated by these results is similar to our qualitative assessment in Fig. 2. We believe it noteworthy that such a large percentage of the samples in Table 1 yield high C_{fg} values. Such a result is not expected if argon loss in nature and the laboratory were governed by different transport mechanisms or if natural diffusion boundaries were disturbed subsequent to closure. We emphasize that we have made little effort to correct problematic behavior in our calculations. For example, degradation of C_{fg} results when age spectra are so flat that the correlation is affected by analytical errors. Similarly, a highly inappropriate choice of activation energy can distort the form of $\log(r/r_o)$ spectrum.

3.4. Extent of Correlation Predicted by the Multi-diffusion Domain Model

The MDD model interprets the argon released from a K-feldspar as a contribution from a discrete distribution of domains sharing the same activation energy and frequency factor, but with domains of varying effective size and argon concentration (LOVERA et al., 1989). Thus, the shape of the $\log(r/r_o)$ plot is only a function of the domain distribution (i.e., relative sizes, ρ_i , and volume concentrations, ϕ_i) and represents the change in effective retentivity of the sample as smaller domains are progressively outgassed. While the age spectrum also reflects this effect, its form can be significantly influenced by

the details of the thermal history it experienced in nature. For example, linear slow cooling tends to result in sinuous age spectra (Fig. 3a and 3b) that resemble the $\log(r/r_o)$ plot, whereas rapid cooling gives rise to flat age spectra.

Given that the form of the age spectrum in the MDD model represents a convolution of diffusion domain properties and characteristics imposed by the thermal history, cross correlation of model age and $\log(r/r_o)$ spectra are not expected to invariably yield C_{fg} values of unity. Rather a distribution of C_{fg} values approaching unity should be obtained. For linear cooling histories, synthetic age and $\log(r/r_o)$ spectra are expected to yield high correlation regardless of the rate of cooling. This is not the case, however, for complex cooling histories in which the rate of cooling changes significantly throughout the interval during which argon is being retained. The drop in correlation could be significantly greater if reheating is involved in the K-feldspar thermal history. In order to quantify this effect, we have calculated C_{fg} values of synthetic age spectra obtained from a random distribution of thermal histories using a single set of distribution and diffusion parameters determined for N13 K-feldspar. In Fig. 5, we consider both monotonic cooling and thermal histories permitting transient heating (Fig. 5a, and 5b, respectively). In the case of monotonic cooling, cross-correlation values are reduced typically by 2% (Fig. 5c). Greater degradation of C_{fg} occurs in the case of transient heating (Fig. 5d). Dissimilar forms for the age and $\log(r/r_o)$ spectra are anticipated when transient heating over short time scales takes place (MCDUGALL and HARRISON, 1999).

3.5. Comparison of Measured and MDD model results

As demonstrated above, synthetic MDD age and $\log(r/r_o)$ spectra are expected to yield C_{fg} values less than unity. Hence correlation results from spectra calculated from experimental data will not reflect the extent to which principals underlying the MDD model have been upheld unless effects described in section 3.4 are taken into account. We accomplish this by normalizing the experimental C_{fg} values by corresponding values obtained by cross correlating the samples best-fit MDD age and $\log(r/r_o)$ spectra

(Normalized $C_{fg} = \text{Experimental } C_{fg} / \text{MDD model } C_{fg}$). Such normalization removes the degrading effect on the correlation produced by a complex thermal history.

At this point, we wish to eliminate confusion that may exist as to the relationship between the experimental data and best-fit MDD spectra. We emphasize that while the best-fit MDD $\log(r/r_o)$ spectrum generally reproduces the measured $\log(r/r_o)$ results, a close fit of the MDD model age spectrum to the experimental data can only occur for samples that satisfy all the constraints imposed by the MDD model. The most important assumption is that laboratory diffusion properties exhibited by the sample (which are used as a constraint along with the thermal history in calculating the age spectrum) must adequately describe how argon accumulated within the sample in nature. Hence, the extent to which normalized C_{fg} values converge upon unity is a measure of how faithful the MDD model represents natural argon accumulation in K-feldspar.

From our database (Table 1), we have selected a subset of K-feldspars to compare correlation values obtained from experimental results and from the MDD model. Because we were only interested in K-feldspars that could potentially be described by the MDD model, we selected only reasonably well behaved samples (i.e., C_{fg} values above 0.85). To further ensure a valid comparison, only K-feldspars whose interval of correlation was greater than 50% were used (see Table 1). Eighty-five samples satisfied these criteria (Table 2). For simplicity we model all samples assuming slow cooling. Note that this could imply an artificial decrease in the normalized C_{fg} value for samples that experienced transient heating in nature. In calculating $\log(r/r_o)$ plots for the samples in Table 2, we used customized diffusion parameters that were obtained in the manner described by (LOVERA et al., 1997). Comparison of C_{fg} values obtained in this manner with those previously determined for all of the samples using a single set of diffusion parameters ($E=46$ kcal/mol, $\log(D_o/r_o^2)=5$) revealed deviations of less than 1% in most cases. This validates the cruder approach employed in section 3.2.

Cross-correlation results for the experimentally determined age and $\log(r/r_o)$ spectra of the 85 K-feldspars are shown in Fig. 6a. An approximately normal distribution centered upon 0.93 ± 0.03 is

obtained. While this distribution contrasts somewhat from the behavior expected from the MDD model (i.e., highly asymmetric and more tightly clustered distribution skewed towards unity illustrated in Fig. 6b), some deviation is expected to result simply from experimental error in $^{40}\text{Ar}/^{39}\text{Ar}$ analysis. Cumulative frequency distributions for both the laboratory and MDD model C_{fg} values are shown in Fig. 6c. The distribution of experimental C_{fg} values is similar in form to those yielded by the MDD model but is offset by 0.04 correlation units. The normalized distribution of C_{fg} values is represented by the bold curve in Fig. 6c. Note that roughly 60% of the normalized values exceed 0.95 (see Table 2). A deviation of 0.05 from unity appears small given the uncertainties involved in the calculation of the cross-correlation and MDD model fit. Hence we consider that these highly correlated samples (normalized $C_{fg} > 0.95$) firmly adhere to the MDD hypothesis and are the most suitable for modeling. Considerable caution should be employed in interpreting samples that exhibit lower degrees of correlation (normalized $C_{fg} \ll 0.95$) in terms of the MDD model.

4. DISCUSSION

Since argon transport in nature cannot be directly observed, speculation upon what exactly controls the mobility of this trace constituent in geologic materials is necessarily based upon circumstantial evidence. Different approaches based upon examination of microscopic and macroscopic properties have been employed to ascertain the validity of extrapolating laboratory properties to natural behavior. We favor a macroscopic approach based upon examination of the self-consistency of ^{39}Ar laboratory diffusion and $^{40}\text{Ar}/^{39}\text{Ar}$ age systematics supported by comparison with results from other thermochronologic methodologies and independent knowledge of the geologic evolution of the region under study. Our motivation to draw conclusions based upon analysis of bulk properties and study of large numbers of samples is rooted in the macroscopic nature of the MDD model and the recognition that it may be ill posed to serve as a microstructural probe. While there is no *a priori* requirement that argon diffusion domains be directly linked with microstructural properties in order to obtain valid thermal histories (see section 4.2.1), reasonable correspondence has been proposed (FITZ GERALD and

HARRISON, 1993). Based upon systematic study of large numbers of samples, we have concluded that the argon retention properties of the majority of K-feldspars are well-described by the MDD model (LOVERA et al., 1997).

An alternative viewpoint has emerged among researchers who have examined microscopic images of a small number of generally anomalous samples and asserted that the MDD model is not a viable method for determining crustal thermal histories from K-feldspar $^{40}\text{Ar}/^{39}\text{Ar}$ step-heating results (ARNAUD and KELLEY, 1997; BURGESS et al., 1992; FOLAND, 1994; PARSONS et al., 1999; PARSONS et al., 1988). Given the relatively common occurrence of clearly problematic samples (Fig. 2), we question the generality of conclusions based upon such limited sampling. Moreover, while microstructural observations can unarguably be made with high resolution, a direct link to bulk $^{40}\text{Ar}^*$ distributions and diffusion properties remains out of reach except potentially in the near surface region where UV laser $^{40}\text{Ar}^*$ depth-profiling methods may be employed (WARTHO et al., 1999).

4.1. Requirements for extracting thermal histories from K-feldspar $^{40}\text{Ar}/^{39}\text{Ar}$ step-heating data

While the postulates of the MDD model have been previously outlined in considerable detail (e.g., (LOVERA et al., 1989), it is worthwhile to reconsider the underlying assumptions in light of the recent discussion of (PARSONS et al., 1999). Their eleven conditions (pg. 93 (PARSONS et al., 1999) for obtaining thermal histories using MDD theory fall into three general categories depending upon how each impact implementation of the model. Their first two requirements (i.e., conservation of diffusion behavior between nature and the laboratory, formation of domains above argon closure) are fundamental. Failure of laboratory-determined properties to adequately mimic those operative in nature would obviously invalidate thermal histories generated by the MDD approach. By comparison, all other issues are of secondary importance. For example, assumptions in the second category (conditions 3 and 4; pg. 93) pertain mainly to how the $^{40}\text{Ar}/^{39}\text{Ar}$ analysis is performed. They represent potential experimental pitfalls that have been tested in the case of K-feldspar and concluded to be insignificant (LOVERA et al., 1993). Moreover, modification of the experimental approach could potentially circumvent deleterious

effects resulting from departure of the assumptions. Similarly, the final class of requirements (conditions 5 to 11; pg. 93) are specific mathematical restrictions imposed on the model to permit representation of argon diffusion behavior in K-feldspar in the simplest possible terms. Specific details of the model, such as geometry and number of domains, are simply mathematical abstractions that have no bearing on thermal history solutions (LOVERA et al., 1991). For example, approximation of a zero boundary condition restricts the relevance of the model to those cases where independent evidence supporting this assumption exists (see section 2.3). The assumption of uniform potassium distribution is not always met but the effect of deviations from this assumption on model predictions are of second order and can be independently addressed (LOVERA et al., 1997). For example, while (TURNER and WANG, 1992) and (BURGESS et al., 1992) interpreted ^{39}Ar loss induced in crushing experiments of authigenic and hypersolvus K-feldspars as indicating that significant $^{39}\text{Ar}_K$ may be derived from non-volume including fluid inclusions, (HARRISON et al., 1993) demonstrated that typical basement K-feldspars contain trivial quantities. (FOLAND, 1994) suggestion that significant $^{40}\text{Ar}^*$ accumulated naturally within isolated micropores could explain certain features of age spectra and Arrhenius data was shown by (LOVERA et al., 1997) to be due to the presence of a small distribution of diffusion domains.

The emphasis of the MDD model is to simplify the parameterization of the problem without compromising the ability of the model to describe the laboratory diffusion characteristics of K-feldspar with sufficient precision so as to be useful in thermal history reconstruction. Further specification of these attributes would add unnecessary degrees of freedom and make parameter estimation and model diffusion predictions more difficult. Throughout our laboratory experiments we found little or no evidence that additional complexity is required to model “well-behaved” (see section 2.3) K-feldspar data.

In the following discussion we examine the consequences of failure of the fundamental assumption that laboratory determined diffusion properties adequately mimic argon retention in K-feldspar during crustal residence. In particular, we deal with assertions that (1) K-feldspar diffusion properties

determined in the laboratory characteristically differ from those prevalent in nature and (2) that the MDD model is an inappropriate representation of natural K-feldspar diffusion properties (LEE, 1995; PARSONS et al., 1999; REDDY et al., 1999).

4.2. What is the influence of low-temperature recrystallization upon thermal history results?

Based largely upon two-feldspar thermometry of K-feldspar microstructural domains that was guided by optical and transmission electron microscopy, it has been claimed that recrystallization at and below ^{40}Ar retention temperatures ($\sim 150\text{-}350^\circ\text{C}$) plays an important role in producing common K-feldspar textural relationships and hence invalidates $^{40}\text{Ar}/^{39}\text{Ar}$ thermochrometry performed with such materials (LEE and PARSONS, 1997; LEE and PARSONS, 1998; PARSONS et al., 1999). We have serious reservations about such broad assertions including whether or not calculated temperatures below ca. 350°C can be considered meaningful when the experimental data used to calibrate alkali feldspar thermometers (e.g., (SMITH and PARSONS, 1974) at these low temperature conditions are subject to considerable uncertainty regarding the attainment of equilibrium due to sluggish reaction rates. Moreover, the complex microstructure that characterize basement K-feldspars generally requires subjective compositional reintegration of exsolved and discrete phases to determine temperatures (FUHRMAN and LINDSLEY, 1988). For example, in the work that (PARSONS et al., 1999) cites to document their claims, not two but four different alkali feldspars are present thus requiring arbitrary assignment of equilibrium pairs (LEE and PARSONS, 1997). Moreover, equilibrium partitioning is far from assured at low temperature even in nature. (LEE and PARSONS, 1997) acknowledge that the accuracy of the low temperature estimates using these geothermometers may be low due to poorly understood effects of ordering and substantial extrapolations outside experimentally-controlled conditions.

As discussed above, the extent of low-temperature ($<350^\circ\text{C}$) reconstitution of K-feldspar is difficult to unambiguously detect and quantify. There is little doubt however, that low-temperature ($<350^\circ\text{C}$) recrystallization, exsolution, or related phenomena could have a marked impact upon diffusion properties of basement K-feldspars. The simplest test involves crushing experiments. For example, crushing

experiments performed by (LOVERA et al., 1993) revealed that reducing the mean particle size of MH-10 K-feldspar from ca. 500 μm (MH-10.bm) to 40 μm (MH-10.g) markedly altered the diffusion behavior of the largest domains and produced a discernable intermediate maxima in the age spectrum (Fig. 7). While crushing to coarser size fractions had no resolvable impact (LOVERA et al., 1993), any process (recrystallization, exsolution, etc.) that affects the largest domains in an analogous manner to MH-10.g in Fig. 7 could adversely affect ability to recover thermal history information if it took place at low enough temperatures. Below we quantitatively explore the impact of instability of the diffusion domains as a function of temperature.

4.2.1. Numerical Simulation of Alteration of the Domain Structure

We have developed a numerical approach to simulate the effect that low temperature recrystallization might have upon recovery of thermal histories using the MDD model. The calculations we perform are quite simple in that they consider only changes to macroscopic properties of the MDD model produced by recrystallization. Although rudimentary, they serve to illustrate the nature of the problem and identify some artifacts that might result from low-temperature recrystallization.

In deciding how best to simulate low-temperature recrystallization, we consider that while diffusion parameters (i.e., activation energy, E , and frequency factor, D_0) might be affected, the first order effect of recrystallization would probably be to alter the nature of the domain distribution (i.e., ρ and ϕ ; in LOVERA et al., 1989). In our calculations we explore a process consistent with exsolution: smaller domains are produced at the expense of larger ones. Since the size range distribution of domains in basement K-feldspar appears relatively constant (LOVERA et al., 1997), the most important effect of this type of recrystallization would likely be to change the relative proportions of the diffusion domains. Accordingly, we fix the range of domain sizes while still permitting the proportions of domains to vary during recrystallization. Argon transport is simulated through the use of a finite difference algorithm based on the Crank-Nicholson implicit method (CRANK, 1975) to describe diffusion through plane slabs with zero boundary conditions.

We have constrained the final domain distribution to resemble that of a typical K-feldspar (LOVERA et al., 1997). As indicated in Table 3, we employ eight domains, a typical quantity indicated by best-fit routines (LOVERA et al., 1997). In our model, recrystallization increases the proportions of the four smallest domains at the expense of the four largest ones. Hence, the overall retentivity of the reconstituted sample is reduced by recrystallization. Daughter domains inherit ^{40}Ar concentrations from their predecessors as follows: A uniform $^{40}\text{Ar}^*$ concentration equivalent to the mean $^{40}\text{Ar}^*$ concentration accumulated within the parent domains is assigned to the daughter domains. Because parent domains in our calculations are 20-50 times larger than daughter domains, use of uniform $^{40}\text{Ar}^*$ concentrations within the newly created domains is justified.

In all calculations, we assumed a linear cooling ($5^\circ\text{C}/\text{m.y.}$) and instantaneous recrystallization at a specified temperature (250, 200, and 150°C). We first performed two different sets of calculations where more than 30% of the samples were affected by recrystallization (models *A* and *B*; see Table 3). The different patterns of recrystallization presented in models *A* and *B* yield end-member results that are distinguished from one another in an important way. Essentially, while model *A* produces age spectra with shapes showing diagnostic features (i.e., intermediate age maxima), the process described in model *B* effectively masks the effects of recrystallization in that it yields age spectra shapes undistinguishable in form from those obtained from unaltered samples. In model *A*, the volume fraction of the smallest domains is increased at the expense of that of the largest domains, that of the second smallest domains increases at the expense of the second largest domains, and so on (see Table 3). This sequence produces a large effect by placing high concentrations of $^{40}\text{Ar}^*$ that accumulated in formerly highly retentive positions into highly unretentive positions. A subtler pattern of recrystallization (largest to fifth largest, second largest to sixth largest, and so on) is adopted in Model *B* (see Table 3).

Age spectra resulting from model *A* recrystallization are shown in Fig. 8a. Curves corresponding to recrystallization at temperatures above 250°C coincide with the age spectrum obtained when no recrystallization has taken place. While the result for 250°C deviates only slightly from the latter, spectra

obtained for 200°C and 150°C recrystallization deviate markedly and exhibit intermediate maxima in their age spectra that clearly signal difficulties for MDD analysis. MDD thermal histories are shown in Fig. 8b. As anticipated from Fig. 8a, the 250°C solution corresponds quite closely to the true thermal history while those obtained for lower temperature recrystallization (200°C and 150°C) underestimate temperatures by up to 100°C. We emphasize that our ability to fit the age spectra produced by low-temperature recrystallization in model A is poor (compare Fig. 8c, 8d and 8e). If we attempted to model such samples at all, we would concentrate only on the lowest temperature portion of the age spectrum where the probability is highest that geologically relevant information could be obtained (see, MAHON et al., 1998).

Results from model B contrast with those from model A in that obviously incongruous features such as the intermediate age maxima are not produced in the age spectrum (contrast Fig. 8a with 8f). Hence no indication of problematic history would be immediately obvious from inspection of the age spectrum and, in the absence of independent evidence for low-temperature recrystallization, thermal history modeling would be performed with such a samples. As in the case of model A, the calculated age spectrum remains largely unaffected when recrystallization occurs at temperatures in excess of 250°C. This is because even when the four smallest domains comprise more than 60% of the sample, they are completely open to argon loss at temperatures beyond 250°C. Breaking the large domains at 250°C produces a change in the age spectrum between 40-70% ³⁹Ar release. This corresponds to the interval of gas release that is dominated by the largest of the smaller domains (*D4*). Although the MDD cooling history obtained from fitting the 250°C result differs from the imposed thermal history by up to 40°C between 30 and 45 Ma, the result converges upon the imposed thermal history below 225°C (Fig. 8f and 8g). Breaking the domain structure at 200°C produces a much larger effect in the age spectrum. The misfit in the recovered thermal history now increases to up to 75°C in the region above 175°C. If reorganization occurs at or below 150°C the entire calculated thermal history is affected by systematic errors (i.e., is shifted to lower temperatures by ~75°C). We note that such an effect would create a

substantial discrepancy between the thermal history calculated from the K-feldspar degassing data and other thermochronometric systems monitoring the same temperature interval such as zircon fission track dating (TAGAMI et al., 1996) or sphene U-Th-He analysis (REINERS and FARLEY, 1999).

It is important to emphasize that the magnitude of the effects described above depends critically upon the extent of recrystallization. To illustrate this, we have performed additional model *B* calculations for recrystallization at 200°C that are presented in Fig. 9. These results indicate that the maximum discrepancy in temperature decreases from ~70°C to ~10°C when the extent of recrystallization is decreased from 32% to 6% (Fig. 9b). Inasmuch as uncertainties in the MDD parameters themselves account for temperature uncertainties of ±20°C or more, small degrees of recrystallization would have negligible impact upon the overall result.

Calculations summarized in Fig. 8 indicate that even substantial recrystallization at temperatures as low as 300°C may have little effect upon ability to recover thermal histories using the MDD approach. Even though the two largest domains in the example were characterized by bulk closure temperatures for Ar loss (337°C and 321°C for *D8* and *D7* respectively) above 300°C, their smaller successors remain open (251°C and 221°C for *D4* and *D3*). Because of this, ⁴⁰Ar* inherited from the large domains is lost before they begin to close. Degradation of the age spectra does not begin to occur until ca. 250°C since bulk closure for the fourth largest domain (251°C) has been attained. In spite of this difficulty, the portion of the thermal history below ca. 225°C is still faithfully recorded since the three smallest domains remain open.

4.2.2. *Implications of Domain Instability Calculations*

The significance of the calculations presented above clearly depends somewhat upon details of the domain distribution and the nature of the recrystallization. Nevertheless, it is reasonable to generalize their significance by stating that substantial recrystallization below 300°C is required to invalidate high-temperature portions of K-feldspar thermal histories obtained from MDD modeling. Although the situation becomes more problematic as significant domain instability occurs at progressively lower

temperatures, we are not aware of any experimental or field-based evidence indicating that large-scale textural and compositional reconstitution is prevalent in typical basement K-feldspars (>85% orthoclase component) at conditions below ca. 300°C. For example, partial replacement of basement K-feldspar to adularia appear to be spatially restricted to crystalline rocks immediately adjacent to basin unconformities (MENSING, 1983) or zones of intense hydrothermal alteration. Textural modifications considered by (PARSONS et al., 1999) appear, in large part, to be higher temperature phenomena. For example, formation of misfit dislocations associated with coarse lamellae in the Shap alkali feldspar described by (PARSONS et al., 1999) as a serious impediment to recovery of thermal histories is interpreted by (LEE and PARSONS, 1997) to form between 410-370°C. Clearly, modifications to the domain structure at such high temperatures are irrelevant since no $^{40}\text{Ar}^*$ accumulates within even the largest domains in this temperature range. (PARSONS et al., 1999) suggest that $^{40}\text{Ar}^*$ might be trapped within dislocations marking these boundaries. However, such a process is unproven and effects ascribed to it (e.g., (FOLAND, 1994) are readily explained by aspects of the MDD model (LOVERA et al., 1997). The role of additional lower temperature processes ((6) thru (8) in PARSONS et al., 1999) in influencing argon transport are quite uncertain, particularly since they appear limited in volumetric importance and occur at unknown (and possibly high) temperature. Moreover renewed albite growth and other recrystallization observed in alkali feldspar within conglomerate derived from the Shap Granite holds little relevance for typical basement K-feldspars ((9) in PARSONS et al., 1999).

It is worthwhile to consider the viability of the MDD model under seemingly unfavorable circumstances. For example, detrital K-feldspar concentrates studied by (MAHON et al., 1998) are clearly polygenetic materials. All exhibit minor ‘humps’ in their age spectra similar in form to that depicted in Fig. 7. Values of $C_{fg}(u)$ obtained for those detrital samples range between 0.80-0.94. In spite of this non-ideal behavior, the diverse thermal histories experienced by individual grains and the burial histories constrained by applying the MDD model were found to be in excellent agreement with independent estimates when analysis was limited to the initial 20% of ^{39}Ar release that corresponded to the common

low-temperature burial history (150-200°C depending upon depth) experienced by the detrital grains throughout the Late Cenozoic (MAHON et al., 1998). This is unsurprising inasmuch as the domains characterizing the initial 20% release in these samples are characterized by low bulk closure temperatures (<150-200°C). Hence, while diagenetic effects and polygenetic evolution could potentially complicate recovery of detrital K-feldspar thermal histories, intra- and intersample consistency checks, direct imaging of authigenic features, and comparison with other thermochronometric systems, would appear to provide sufficient controls to assess these concerns.

4.2. Representation of the volume diffusion process

The MDD model unarguably presents a simplistic representation of the diffusion characteristics of basement K-feldspar. For example, (PARSONS et al., 1999) view alkali feldspars as "a complex assemblage of touching and interacting domains, with a variety of blind and open pathways between them" and emphasize in their Fig. 1 that "real microstructures" are completely dissimilar to the geometry treated by the MDD model. They assert that interpretation of K-feldspar $^{40}\text{Ar}/^{39}\text{Ar}$ data through the use of a fundamentally incorrect argon transport model should necessarily lead to inaccurate thermal histories and alternatively favor the multipath (MP) model (LEE, 1995) which incorporates interaction between heterogeneous diffusion regions as a superior description of argon transport within K-feldspar. Such reasoning does not take into account that it is not presently possible to verify by direct observation the influence of any microstructural feature upon argon mobility in K-feldspar. Moreover, it should be noted that experimental studies (ARNAUD and KELLEY, 1997) have demonstrated that the MP model cannot be successfully applied to describe argon diffusion data from basement K-feldspar without modifying the model to such an extent (i.e., eliminating interaction between regions of contrasting diffusion properties) that it is mathematically indistinguishable from the MDD model. In spite of these problems, the arguments of (PARSONS et al., 1999) raise an important question: How important is the nature of the diffusion model when the goal is recovery of thermal history information?

To address this issue, we have developed a conceptually different diffusion model (the heterogeneous diffusion or HD model) based upon a continuous variation of diffusion properties with no intracrystalline diffusion boundaries present. In developing the HD model, our goal has not necessarily been to obtain a superior representation of K-feldspar diffusion properties, but rather to test the ability of the MDD model to act as a proxy for a radically different diffusion mechanism and still produce an accurate estimation of the thermal history experienced by the sample.

4.2.1. *The Heterogeneous Diffusion (HD) Model*

The heterogeneous diffusion model assumes that diffusion properties of a sample can be described by a spatially dependent pre-exponential factor, $D_o(\mathbf{x})$. The temperature dependence of the diffusion coefficient $D(x,T)$ is represented by the Arrhenius equation:

$$D(x,T) = D_o(x)e^{-E/RT} \quad (5)$$

The HD and MDD models differ in a fundamental way. Specifically, argon is released only from the external boundaries of HD crystals because no intracrystalline diffusion boundaries (such as that potentially provided by perthite lamellae boundaries) exist. Note that two assumptions of the MDD model, (i.e., the zero boundary condition and no-interactions between domains) do not apply to the HD model. In principle, the pre-exponential factor $D_o(x)$ could be represented by any continuous function of x . However, the range of functions that are capable of reproducing K-feldspar argon diffusion characteristics observed in the laboratory is restricted. For example, the $D_o(x)$ function shown in the inset of Fig. 10a produces the characteristic Arrhenius behavior of most K-feldspars (LOVERA et al., 1997). As shown, the HD model is able to successfully mimic important aspects of basement K-feldspar ³⁹Ar diffusion behavior (i.e., kink in the Arrhenius plot and systematic lowering of diffusion properties during progressive temperature cycling, Fig. 10a). Note how retentivity barriers affect the overall release of argon. The highly retentive interior ($-0.2 < x < 0.2$) and the two symmetric wells of intermediate retentivity (at $x = \pm 0.6$) produce the classic sinuous behavior of age and $\log(r/r_o)$ spectra exhibited by basement K-feldspar (Fig. 10b). In terms of the MDD model, the $\log(r/r_o)$ spectrum in Fig. 10b would be

interpreted as being dominated by ^{39}Ar release from three discrete domain sizes (inset to Fig. 10b; see (LOVERA et al., 1991). However, this interpretation completely misrepresents the intrinsic physical properties of the HD crystal (i.e., intrinsic diffusion length scales inferred by the MDD model lack a meaningful counterpart in the HD model).

4.2.2. *Implications for Thermochronology*

Can the MDD model accurately recover thermal history information from a sample with the diffusion characteristics assumed in the HD model? To test this, we have imposed a thermal history upon the HD crystal described above. Fig. 10c shows the 90% confidence intervals of a distribution of 50 best-fit cooling histories calculating by interpreting the age and $\log(r/r_o)$ spectra of the HD crystal with the MDD model. As shown in Fig. 10c, the MDD model faithfully reproduces the input $T-t$ history in the interval of sample closure (20-55 Ma, 150-300°C). This strongly implies that recovery of thermal history information is essentially independent of the formulation of the model provided that thermally activated volume diffusion is the rate limiting transport mechanism for argon. While this result also implies that estimates of diffusion length scales yield by MDD analysis could be incorrect, we do not view this as a serious shortcoming of a macroscopic model. Our view is that the MDD model is fundamentally a tool to recover thermal histories rather than a probe to reveal details of feldspar microstructure.

5. CONCLUDING REMARKS

The high degree of correlation exhibited between measured age and $\log(r/r_o)$ spectra determined for the majority of K-feldspars we have analyzed validates extrapolation of experimentally determined diffusion properties to conditions attending natural argon loss within the crust. Our experimental results and numerical analysis indicate that the MDD model, while potentially not a sensitive probe of K-feldspar microstructure, can be a robust tool to recover thermal histories. Despite this, a considerable number of basement K-feldspars that are routinely analyzed by the step-heating method yield $^{40}\text{Ar}/^{39}\text{Ar}$ systematics that is clearly problematic for thermal history analysis. The potential of encountering problematic samples must be borne in mind when setting out to apply the approach.

It is well understood that igneous and high-grade metamorphic K-feldspars from mid- to deep-crustal, basement terranes that are targeted for thermal history studies have generally experienced a complex microstructural evolution (e.g.,(BROWN, 1994). Moreover it is reasonable to assume that extensive textural reconstitution of K-feldspar at or below temperatures at which $^{40}\text{Ar}^*$ is retained would have consequences for efforts to recover thermal histories from laboratory measurements. It is essential to bear in mind, however, the temperature range that is relevant to the discussion. $^{40}\text{Ar}/^{39}\text{Ar}$ step-heating experiments performed with K-feldspar (LOVERA et al., 1997) consistently indicate that the onset of argon retention occurs below 350°C and that K-feldspars are essentially closed with respect to argon loss below about 125-175°C. Hence only recrystallization, exsolution, and any other modification to basement K-feldspar that occurs below 350°C is potentially capable of significantly affecting K-feldspar $^{40}\text{Ar}^*$ thermochronology, depending upon the extent of the alteration. Accordingly, higher temperature modification to K-feldspar is irrelevant for thermochronologic considerations involving this phase. We further distinguish any volumetrically significant reconstitution of basement K-feldspar taking place below 150°C as a process that could seriously impair our ability to reconstruct the sample thermal history.

A strength of the MDD model is the fact that a faithful depiction of the intrinsic structure of the feldspar is not required to produce accurate thermochronological results. This was highlighted by the ability of the MDD approach to recover thermal histories from HD crystals. Our fundamental premise is that the most informed opinion regarding the argon transport behavior in a solid comes from interrogation of the migrating argon molecule itself. Assertive arguments regarding the influence of feldspar microstructure on argon diffusion are substantially less valuable in this regard, particularly if they are contradicted by empirical results. The most important piece of information we can obtain in establishing meaningful thermal histories is the loss of argon as a function of temperature and time during laboratory treatment. With these data, progressively more and more complex transport models can be tested until one is found that explains all the observations with the minimum of assumptions. Our

work to date indicates that the MDD model satisfactorily accounts for the vast majority of $^{40}\text{Ar}/^{39}\text{Ar}$ data obtained from basement K-feldspars.

Acknowledgements. This research was conducted under the auspices of Department of Energy grant DE-FG-03-89ER14049. We thank the numerous analysts involved in generating the $^{40}\text{Ar}/^{39}\text{Ar}$ data reported in this paper and the assistance of Nyssa Roeth, Ainslie Harrison, and Natalí Degradi for their help in compiling the database.

REFERENCES

- Arnaud N. O. and Eide E. A. (2000) Brecciation-related argon redistribution in alkali feldspars: An in naturo crushing study. *Geochim. Cosmochim. Acta* **64**(18), 3201-3215.
- Arnaud N. O. and Kelley S. P. (1997) Argon behavior in gem-quality orthoclase from Madagascar: Experiments and consequences for $^{40}\text{Ar}/^{39}\text{Ar}$ geochronology. *Geochim. Cosmochim. Acta* **61**, 3227-3255.
- Baldwin S. L., Harrison T. M., and Fitzgerald J. D. (1990) Diffusion of ^{40}Ar in metamorphic hornblende. *Cont. Mineral. Petrol.* **105**, 691-703.
- Berger G. W. and York D. (1981) Geothermometry from $^{40}\text{Ar}/^{39}\text{Ar}$ dating experiments. *Geochim. Cosmochim. Acta* **45**(6), 795-811.
- Brown W. L. (1994) Feldspar in igneous rock. In *Feldspar and their Reactions*, Vol. NATO ASI 421 (ed. I. Parsons), pp. 449-499. Kluwer, The Netherlands.
- Burgess R., Kelley S. P., Parsons I., Walker F. D. L., and Worden R. H. (1992) ^{40}Ar - ^{39}Ar analysis of perthite microstructures and fluid inclusions in alkali feldspars from the Klokken syenite, South Greenland. *Earth Planet. Sci. Lett* **109**, 147-167.
- Crank J. (1975) *The Mathematics of Diffusion*. Oxford University Press.
- Fitz Gerald J. D. and Harrison T. M. (1993) Argon diffusion domains in K-feldspar I: Microstructures in MH-10. *Contrib. Mineral. Petrol.* **113**, 367-380.
- Foland K. A. (1974) ^{40}Ar diffusion in homogeneous orthoclase and an interpretation of Ar diffusion in K-feldspars. *Geochim. Cosmochim. Acta* **38**, 151-166.
- Foland K. A. (1994) Argon Diffusion in Feldspars. In *Feldspars and Their Reactions*, Vol. 421 (ed. I. Parsons), pp. 415-447. Kluwer Academic.

- Foster D. A., Harrison T. M., Copeland P., and Heizler M. T. (1990) Effects of excess argon within large diffusion domains of K-feldspar age spectra. *Geochim. Cosmochim. Acta* **54**, 1699-1708.
- Frankel A. and Clayton R. W. (1986) Finite difference simulations of seismic scattering; implications for the propagation of short-period waves in the crust and models of crustal heterogeneity. *J. Geophys. Res.* **91**, 6465-6489.
- Fuhrman M. L. and Lindsley D. H. (1988) Ternary-feldspar modeling and thermometry. *Am. Mineral.* **73**(3-4), 201-215.
- Giletti B. J. (1974) Studies in diffusion I: Argon in phlogopite mica. In *Geochemical transport and kinetics*, Vol. 634 (ed. A. W. Hofmann, B. J. Giletti, H. S. Yoder, Jr., and R. A. Yund), pp. 107-115. Carnegie Institution of Washington Publication.
- Girard J. P. and Onstott T. C. (1991) Application of $^{40}\text{Ar}/^{39}\text{Ar}$ laser probe and step-heating techniques to the dating of authigenic K-feldspar overgrowths. *Geochim. Cosmochim. Acta* **55**, 3777-3793.
- Grove M. and Bebout G. E. (1995) Cretaceous tectonic evolution of coastal southern California: Insights from the Catalina Schist. *Tectonics* **14**, 1290-1308.
- Grove M. and Harrison T. M. (1996) $^{40}\text{Ar}^*$ diffusion in Fe-rich biotite. *Am. Mineral.* **81**(7-8), 940-951.
- Harrison T. M. (1990) Some observations on the interpretation of feldspar $^{40}\text{Ar}/^{39}\text{Ar}$ results. *Isotope Geosci.* **80**, 219-229.
- Harrison T. M., Duncan I., and McDougall I. (1985) Diffusion of ^{40}Ar in biotite: Temperature, pressure and composition effects. *Geochim. Cosmochim. Acta* **49**, 2461-2468.
- Harrison T. M., Heizler M. T., and Lovera O. M. (1993) In vacuo crushing experiments and K-feldspar thermochronometry. *Earth Planet. Sci. Lett.* **117**, 169-180.
- Harrison T. M., Heizler M. T., Lovera O. M., Chen W., and Grove M. (1994) A chlorine disinfectant for excess argon released from K-feldspar during step-heating. *Earth Planet. Sci. Lett.* **123**, 95-104.
- Harrison T. M. and McDougall I. (1981) Excess ^{40}Ar in metamorphic rocks from Broken Hill, New South Wales: Implications of $^{40}\text{Ar}/^{39}\text{Ar}$ age spectra and the thermal history of the region., *Earth Planet. Sci. Lett.* **55**, 123-149.
- Harrison T. M., Yin A., Grove M., Lovera O. M., and Ryerson F. J. (2000) The Zedong Window: A record of superposed Tertiary convergence in southeastern Tibet. *Journal of Geophysical Research, B, Solid Earth and Planets* **105**, 19211-19230.
- Kastner M. and Siever R. (1979) Low temperature feldspars in sedimentary rocks. *Am. J. Sci.* **279**(4), 435-479.

- Kelley S. P., Arnaud N. O., and Turner S. P. (1994) High-Spatial-Resolution $^{40}\text{Ar}/^{39}\text{Ar}$ Investigation using an Ultra-Violet Laser Probe Extraction Technique. *Geochim. Cosmochim. Acta* **58**(16), 3519-3525.
- Lee J. K. W. (1995) Multipath diffusion in geochronology. *Contrib. Mineral. Petrol.* **120**, 60-82.
- Lee J. K. W., Onstott T. C., Cashman K. V., Cumbest R. J., and Johnson D. (1991) Incremental heating of hornblende in vacuo; implications for $^{40}\text{Ar}/^{39}\text{Ar}$ geochronology and the interpretation of thermal histories. *Geology* **19**(9), 872-876.
- Lee M. R. and Parsons I. (1997) Dislocation formation and albitization in alkali feldspars from the Shap granite. *Am. Mineral.* **82**, 557-570.
- Lee M. R. and Parsons I. (1998) Microtextural controls of diagenetic alteration of detrital alkali feldspar: A case study of the Shap conglomerate (lower carboniferous), Northwest England. *J. Sediment. Res.* **68**(1), 198-211.
- Lovera O. M., Grove M., Harrison T. M., and Mahon K. I. (1997) Systematic analysis of K-feldspar $^{40}\text{Ar}/^{39}\text{Ar}$ step heating results: I. Significance of activation energy determinations. *Geochim. Cosmochim. Acta* **61**(15), 3171-3192.
- Lovera O. M., Heizler M. T., and Harrison T. M. (1993) Argon diffusion domains in K-feldspar II: kinetic properties of MH-10. *Contrib. Mineral. Petrol.* **113**, 381-393.
- Lovera O. M., Richter F. M., and Harrison T. M. (1989) The $^{40}\text{Ar}/^{39}\text{Ar}$ thermochronometry for slowly cooled samples having a distribution of diffusion domain sizes. *J. Geophys. Res.* **94**, 17917-17935.
- Lovera O. M., Richter F. M., and Harrison T. M. (1991) Diffusion domains determined by ^{39}Ar released during step heating. *J. Geophys. Res.* **96**, 2057-2069.
- Mahon K. I., Harrison T. M., and Grove M. (1998) The thermal and cementation histories of a sandstone petroleum reservoir, Elk Hills, California. Part I: $^{40}\text{Ar}/^{39}\text{Ar}$ thermal history results. *Chem. Geol.* **152**, 227-256.
- McDougall I. and Harrison T. M. (1999) *Geochronology and Thermochronology by the $^{40}\text{Ar}/^{39}\text{Ar}$ Method*. Oxford University Press.
- Mensing T. M., and Faure, G. (1983) Identification and age of neofomed Paleozoic feldspar (adularia) in a Precambrian basement core from Scioto County, Ohio, USA. *Contrib. Mineral. Petrol.* **82**(4), 327-333.
- Onstott T. C., Phillips D., and Pringle-Goodell L. (1991) Laser microprobe measurement of chlorine and argon zonation in biotite. *Chem. Geol* **90**, 145-168.

- Parsons I., Brown W. L., and Smith J. V. (1999) $^{40}\text{Ar}/^{39}\text{Ar}$ thermochronology using alkali feldspars; real thermal history or mathematical mirage of microtexture? *Contrib. Mineral. Petrol.* **136**(1-2), 92-110.
- Parsons I., Rex D. C., Guise P., and Halliday A. N. (1988) Argon-loss by alkali feldspar. *Geochim. Cosmochim. Acta* **52**, 1097-1112.
- Press W. H., Fannery B. P., Teukolsky S. A., and Vetterling W. T. (1988) *Numerical Recipes: The Art of Scientific Computing*. Cambridge University Press.
- Quidelleur X., Grove M., Lovera O. M., Harrison T. M., Yin A., and Ryerson F. J. (1997) Thermal evolution and slip history of the Renbu Zedong thrust, southeastern Tibet. *J. Geophys. Res.* **102**, 2659-2679.
- Reddy S. M., Potts G. J., Kelley S. P., and Arnaud N. O. (1999) The effects of deformation-induced microstructures on intragrain $^{40}\text{Ar}/^{39}\text{Ar}$ ages in potassium feldspar. *Geology* **27**, 363-366.
- Reiners P. W. and Farley K. A. (1999) Helium diffusion and (U-Th)/He thermochronometry of titanite. *Geochim. Cosmochim. Acta* **63**(22), 3845-3859.
- Richter F. M., Lovera O. M., Harrison T. M., and Copeland P. (1991) Tibetan tectonics from $^{40}\text{Ar}/^{39}\text{Ar}$ analysis of a single K-feldspar sample. *Earth Planet. Sci. Lett.* **105**, 266-278.
- Smith P. and Parsons I. (1974) The alkali feldspar solvus at 1 kilobar water-vapor pressure. *Mineralogical Magazine and Journal of the Mineralogical Society* **39**(307), 747-767.
- Tagami T., Carter A., and Hurford A. J. (1996) Natural long-term annealing of the zircon fission-track system in Vienna Basin deep borehole samples; constraints upon the partial annealing zone and closure temperature. *Chem. Geol.* **130**(1-2), 147-157.
- Telford W. M., Geldart L. P., and Sheriff R. E. (1990) *Applied geophysics*. Cambridge University Press.
- Turner G. and Wang S. (1992) Excess argon, crustal fluids and apparent isochrons from crushing K-feldspar. *Earth. Planet. Sci. Lett.* **110**, 193-211.
- Villa I. M. (1994) Multipath Ar transport deduced from isothermal heating experiments. *Earth. Planet. Sci. Lett.* **122**(3-4), 393-401.
- Villa I. M., Pearce, J.A. (1990) Geochronology and excess Ar geochemistry of the Lhotse Nup Leucogranite, Nepal Himalaya. *Journal of Volcanology and Geothermal Research* **44**(1-2), 89-103.
- Warnock A. C. and van de Kamp P. C. (1999) Hump-shaped $^{40}\text{Ar}/^{39}\text{Ar}$ age spectra in K-feldspar and evidence for Cretaceous authigenesis in the Fountain Formation near Eldorado Springs, Colorado. *Earth. Planet. Sci. Lett.* **174**(1-2), 99-111.

- Wartho J. A. (1995) Apparent argon diffusive loss $^{40}\text{Ar}/^{39}\text{Ar}$ age spectra amphiboles. *Earth. Planet. Sci. Lett.* **134**, 393-407.
- Wartho J. A., Kelley S. P., Brooker R. A., Carroll M. R., Villa I. M., and Lee M. R. (1999) Direct measurement of Ar diffusion profiles in a gem-quality Madagascar K-feldspar using the ultra-violet laser ablation microprobe (UVLAMP). *Earth. Planet. Sci. Lett.* **170**(1-2), 141-153.
- Zeitler P. K. and FitzGerald J. F. (1986) Saddle-shaped $^{40}\text{Ar}/^{39}\text{Ar}$ age spectra from young, microstructurally complex potassium-feldspars. *Geochim. Cosmochim. Acta* **50**, 1185-1199,.

Figure Captions

Figure 1. (a) Examples of K-feldspar age spectra typical of those employed in thermal history studies.

All samples from adjacent the Renbu-Zedong thrust, southern Tibet (QUIDELLEUR et al., 1997). Note that the initial low-temperature portions of the age spectra have been corrected for Cl-correlated excess radiogenic ^{40}Ar ($^{40}\text{Ar}_E$) as described by (HARRISON et al., 1994). (b) Examples of K-feldspar age spectra that are heavily contaminated with $^{40}\text{Ar}_E$. No corrections for low-temperature Cl-correlated $^{40}\text{Ar}_E$ have been performed. All samples shown are from Zanscar Shear Zone, India. Note the characteristic U-shaped pattern (ZEITLER and FITZGERALD, 1986). Geologically meaningful ages are obtained only between 15-35% cumulative % ^{39}Ar release. (c) Examples of K-feldspar age spectra that exhibit intermediate age maxima. Sample B2 consists of detrital K-feldspar overgrown and partially replaced by sanidine structure adularia from Brazil (GIRARD and ONSTOTT, 1991). Sample 96-8-22-4a is a K-feldspar from a strongly sheared setting adjacent to the Altyn Taugh fault in Tibet.

Figure 2. (a) Frequency of occurrence of well-behaved and problematic K-feldspar age spectra. (b)

Histogram indicating variation in the portion of K-feldspar age spectra that is affected by low-temperature $^{39}\text{Ar}_E$ contamination. (c) Histogram indicating variation in the % ^{39}Ar released below melting. (d) Histogram indicating variation in the resulting portion of K-feldspar age spectra available for thermal history analysis.

Figure 3. Examples of age and $\log(r/r_o)$ spectra we have examined with our correlation algorithms. The

portion of the spectra for which we have performed calculations is indicated in black. Correlation values, C_{fg} , are indicated on the figures. Filled gray symbols represent the crossover points x_f and x_g (see text for explanation). (a)-(b) Examples of highly correlated K-feldspar age and $\log(r/r_o)$ spectra. Note that the values of x_f and x_g are nearly coincident for both spectra. Samples N-12 and N-13 are coexisting K-feldspars from hanging wall of Gangdese Thrust, Tibet (HARRISON et al., 2000). (c-d) Examples of moderately to poorly correlated K-feldspar age and $\log(r/r_o)$ spectra. Note that the value

of C_{fg} decreases as the values of x_f and x_g diverge. (e-f) Examples of correlation results from K-feldspars with intermediate age maxima. Correlation coefficients are diminished even when the values of x_f and x_g are nearly equal. (g-h) Examples of poorly correlated age and $\log(r/r_o)$ spectra from hydrous phases that decompose during in vacuo heating. Correlation results from 8-1-22 phengite (GROVE and BEBOUT, 1995), and 76-618 hornblende (WARTHON, 1995) illustrate progressive degradation of C_{fg} as natural and experimental argon loss processes become more dissimilar (see text).

Figure 4. Cross-correlation results from K-feldspars listed in Table 1. $\log(r/r_o)$ plots were calculated using a single mean reference line previously determined by Lovera et al. (1997). (a) Cumulative counts of the correlation values, C_{fg} ; (b) Histogram of the C_{fg} values. Note the C_{fg} values of K-feldspars depicted in Fig. 1 and 3.

Figure 5. Predicted variation of C_{fg} values from K-feldspar analyzed by the multi-diffusion domain (MDD) model when nonlinear thermal histories are considered. Diffusion properties used in calculations are those of N13 K-feldspar (HARRISON et al., 2000); (a) randomly generated monotonic cooling histories used in analysis; (b) randomly generated thermal histories involving transient heating; (c) histogram of C_{fg} values produced from randomly generated monotonic cooling histories; (d) histogram of C_{fg} values produced from randomly generated thermal histories involving transient heating.

Figure 6. (a) Histogram of C_{fg} values from Table 2 that were calculated for a subset of 85 K-feldspars selected for detailed analysis (see text for selection criteria). Individual diffusion parameters calculated as described in (LOVERA et al., 1997) were used to construct the $\log(r/r_o)$ plots. (b) Histogram of C_{fg} values for best-fit age and $\log(r/r_o)$ spectra produced by the MDD model when it was employed to calculate monotonic thermal histories for the samples. (c) Cumulative counts of results from (a) and (b) above. The bold curve represents the normalized experimental values (i.e., experimental C_{fg} values divided by the C_{fg} values that result from best-fit age and $\log(r/r_o)$ spectra

produced by application of the MDD model). The parallelism of the experimental and MDD cumulative frequency curves indicate that much of the deviation of experimental C_{fg} values from unity can be attributed to details of the thermal histories experienced by the samples.

Figure 7. Effect of extreme particle size reduction in crushing experiments performed with MH-10 K-feldspar (LOVERA et al., 1993). The mean particle sizes of MH-10.bm and MH-10.g are 500 μm and 40 μm respectively. Note the intermediate age maximum in the age spectra of MH-10.g and its absence in the coarser sample. An equally significant change in the $\log(r/r_o)$ spectra indicate that crushing MH-10 K-feldspar to 40 μm has also altered its diffusion properties. These changes in the age and $\log(r/r_o)$ spectra cause C_{fg} to be reduced from 0.93 to 0.70.

Figure 8. Simulation of the effect of alteration of the domain reorganization at progressively lower temperatures. (a) Age spectra from model A calculations (see text for details). Solutions above 250°C conform to the case of no recrystallization; (b) Thermal histories calculated from multi-diffusion domain analysis of the model A age spectra; (c)-(e) MDD fits to age spectra produced in model A; (f) Age spectra from model B calculations; (g) Thermal histories calculated from multi-diffusion domain analysis of the model B age spectra; (h)-(j) MDD fits to age spectra produced in model B.

Figure 9. Effect of varying the extent of recrystallization in model B at 200°C. (a) Age spectra resulting from 0-30% recrystallization. (b) Thermal histories obtained by applying MDD model.

Figure 10. (a) Arrhenius properties of a heterogeneous diffusion (HD) crystal that exhibits ^{39}Ar diffusion properties similar to those observed for basement K-feldspar. Inset shows the $D_o(x)$ function that describes the spatially variable diffusion properties of the crystal; (b) Age and $\log(r/r_o)$ spectra of the HD crystal. The age spectrum was obtained by assuming the cooling history indicated by the black line in (c) below. The MDD distribution parameters obtained by modeling the $\log(r/r_o)$ spectrum are shown in the inset. Note that the HD model successfully predicts the sinuous, correlated behavior of age and $\log(r/r_o)$ spectra that are characteristic of basement K-feldspars; (c) Thermal history

calculated from the age and ^{39}Ar diffusion properties of the HD crystal using the MDD model approach. Despite the highly inaccurate MDD representation of the argon diffusion properties of the HD crystal (compare insets in (a) and (b) above), the imposed thermal history is recovered with high fidelity.

Table 1. Database samples

SAMPLE NAME	Excess $^{40}\text{Ar}^*$		Int. Age Max	^{39}Ar correlated		C_{fg} (raw)	SAMPLE NAME	Excess $^{40}\text{Ar}^*$		Int. Age Max	^{39}Ar correlated		C_{fg} (raw)
	$^{\text{i}}$ Low T	High T		$^{\text{i}}$ Low limit	$^{\text{iii}}$ High limit			Low T	High T		Low limit	High limit	
26190	x			0.20	0.81	0.54	CM3-62-1E				0.10	0.45	0.91
3790	x		x	0.22	0.71	0.97	CM3-65-2	x			0.12	0.54	0.96
487	x	x		0.17	0.86	0.92	CM3-67-1B	x			0.14	0.53	0.98
489	x	x	x	0.30	0.85	0.81	CM3-70-1B	x			0.11	0.45	0.94
5490	x		x	0.11	0.95	0.65	CP128				0.02	0.83	0.95
5990	x			0.24	0.76	0.71	CV				0.00	0.68	0.96
627				0.09	0.88	0.96	DC10C			x	0.09	0.91	0.89
639KRX				0.01	0.72	0.92	DC2A				0.04	0.97	0.93
6790	x		x	0.37	0.75	0.82	DL3				0.06	0.62	0.98
763A				0.01	0.93	0.65	DSC				0.02	0.86	0.96
798B			x	0.10	0.78	0.63	EH-29R-A1		x		0.13	0.62	0.39
903T4				0.06	0.70	0.81	EH-29R-A2		x		0.07	0.50	0.64
927		x	x	0.01	0.67	0.83	EH-29R-A3		x		0.08	0.55	0.30
93-NG-39				0.01	0.69	0.99	EH-29R-A4		x		0.09	0.56	0.41
940		x		0.09	0.91	0.91	ET194				0.01	0.46	0.99
94-9-12(3)	x			0.18	0.90	0.77	F185				0.04	0.96	0.93
94-9-15(2)	x	x		0.16	0.77	0.52	F188				0.02	0.98	0.91
94-9-8(3)	x	x		0.11	0.75	0.38	F223	x			0.18	0.89	0.93
95-6-11(3)				0.09	0.52	0.72	FA1K	x	x		0.13	0.60	0.67
95-6-12A	x	x		0.25	0.78	0.78	FA21K				0.08	0.52	0.35
96-8-22-4A		x		0.02	0.82	0.30	FA41K				0.05	0.70	0.08
96-9-24-14A	x			0.10	0.49	0.92	FA5K				0.03	0.86	0.84
96-9-24-16		x		0.05	0.82	0.78	FA7K	x			0.15	0.55	0.51
96-MX-001	x			0.16	0.51	0.94	FA8K				0.01	0.91	0.82
96-MX-005				0.04	0.82	0.97	FA9K			x	0.08	0.81	0.71
96-MX-012		x		0.01	0.46	0.77	FF52-32-ST2				0.03	0.57	0.62
97-7-21-6B	x			0.15	0.59	0.58	FO-230	x			0.12	0.54	0.97
97-7-3-3B	x			0.12	0.50	0.80	FO-82	x			0.20	0.58	0.89
97AK101	x			0.19	0.57	0.95	GDC-5-7800		x		0.09	0.83	0.45
97AK102	x			0.16	0.47	0.67	GR04				0.01	0.78	0.90
97AK103				0.08	0.46	0.86	GR11				0.03	0.81	0.92
97AK104		x		0.08	0.74	0.27	GR12	x			0.25	0.90	0.94
98-5-23-2	x			0.24	0.62	0.93	GR13				0.06	0.80	0.91
98-5-23-3	x			0.13	0.60	0.90	GR14				0.02	0.83	0.91
98-5-23-7	x	x		0.23	0.55	0.73	GR15	x			0.11	0.89	0.94
98-5-23-8	x		x	0.19	0.54	0.87	GR16	x			0.13	0.68	0.88
98-8-20-2	x			0.14	1.00	0.65	GR18				0.02	0.85	0.94
98-8-21-2A	x			0.21	0.78	0.95	GR19				0.03	0.90	0.96
98-8-25-7A		x		0.09	0.87	0.44	GR20				0.02	0.84	0.95
98-8-26-6B	x		x	0.22	0.95	0.75	JU	x	x		0.10	0.91	0.83
98-8-9-5		x		0.02	0.89	0.96	KAIL2K	x			0.15	0.77	0.91
98-8-9-6				0.08	0.95	0.97	LF-23-RD-1	x			0.13	0.59	0.77
99-7-26-1B	x	x	x	0.15	0.82	0.36	MCA994KF				0.05	0.69	0.97
AC				0.01	0.69	0.91	MH8911		x		0.02	0.98	0.72
ALB-1		x		0.04	0.63	0.48	MH8913K		x		0.02	0.82	0.73
ANG-1-11400	x			0.18	0.92	0.65	MH8914K				0.05	0.67	0.94
ANG-1-11440			x	0.08	0.94	0.40	MH8915K	x			0.12	0.59	0.51
BW2				0.01	0.64	0.83	MH8916				0.06	0.76	0.71
CARARA			x	0.02	0.94	0.83	MH8926				0.02	0.85	0.84
CB2493KF				0.02	0.72	0.96	MH8932K	x			0.15	0.83	0.79
CG194				0.02	0.74	0.95	MH897K		x		0.05	0.71	0.73
CH-17	x			0.18	0.90	0.77	MN1				0.07	0.71	0.94
CH-26B		x		0.01	0.71	0.47	MN7				0.02	0.65	0.91
CH-27		x		0.01	0.35	0.85	MP17				0.05	0.74	0.97
CH-29A	x			0.27	0.49	0.93	MP				0.01	0.81	0.84
CH-29C	x	x		0.10	1.00	0.51	N10				0.05	0.81	0.97
CH-29D	x			0.24	0.56	0.74	N11				0.04	0.82	0.95
CH-29G	x			0.19	0.38	0.82	N12	x			0.15	0.84	0.98
CH-3		x		0.02	0.64	0.27	N13	x			0.12	0.83	0.98
CH-30	x			0.15	0.98	0.94	N14				0.10	0.87	0.97
CLBB19KF				0.07	0.87	0.90	N15A				0.07	0.77	0.83
CM1				0.02	0.64	0.90	N16	x			0.14	0.79	0.99
CM3-60-1B		x		0.09	0.38	0.94	N17A	x			0.17	0.99	0.87

SAMPLE NAME	Excess $^{40}\text{Ar}^*$		Age Max	^{39}f correlated		C_{fig} (raw)
	Low T	High T		Low limit	High limit	
N19	x			0.14	0.61	0.91
N21	x			0.10	0.94	0.90
N25	x	x		0.10	0.79	0.84
N5				0.07	0.69	0.96
N6	x			0.10	0.66	0.98
N8	x			0.10	0.80	0.96
N9				0.03	0.87	0.95
NG17				0.01	0.66	0.94
NG37				0.05	0.75	0.96
NG6				0.02	0.66	0.91
PN794				0.05	0.59	0.98
PN-995				0.01	0.80	0.88
PP1	x			0.10	0.75	0.96
PRP86		x		0.07	0.77	0.53
QH1				0.05	0.60	0.96
QH-3				0.04	0.83	0.91
SA4092KF				0.06	0.73	0.82
SEM394KF				0.02	0.85	0.94
SEM694KF				0.07	0.76	0.99
SFH		x		0.02	0.79	0.91
SJ394				0.04	0.65	0.94
SL1				0.05	0.73	0.80
SM11				0.05	0.59	0.86
SP133A				0.05	0.44	0.95
SP138				0.04	0.38	0.87
SP20		x		0.03	0.38	0.33
SP				0.03	0.83	0.85
SY				0.04	0.79	0.94
TR-2		x		0.02	0.99	0.22
TR210	x			0.10	0.81	0.87
TR83				0.08	1.00	0.84
TRBB86				0.01	0.91	0.96
TS1		x		0.01	0.90	0.00
V103KF				0.05	1.00	0.88
V12KF	x	x		0.20	0.85	0.86
V-132	x	x		0.14	0.54	0.08
V1KF	x	x		0.10	0.93	0.63
V4KF		x		0.06	0.84	0.86
XH10B2K	x		x	0.15	0.99	0.49
YA24				0.03	0.63	0.94
YAN11				0.04	0.61	0.96
YANS1				0.05	0.78	0.97
YANS-6				0.05	0.75	0.97
YN27				0.03	0.75	0.93
<i>YU36K</i>				0.02	0.98	0.35
<i>YU38K</i>	x	x		0.20	0.84	0.87
<i>YU39K</i>				0.05	0.84	0.15
<i>YU40K</i>	x			0.18	0.59	0.83
<i>YU56K</i>	x			0.12	0.82	0.65
<i>YU57</i>	x			0.12	0.77	0.70
<i>YU62</i>	x			0.12	0.76	0.63
<i>YU94K</i>	x			0.15	0.63	0.90
<i>YU97K</i>	x			0.12	0.76	0.95
<i>YX16K</i>				0.02	0.73	0.84
<i>YX29K</i>				0.04	0.83	0.64
<i>YX41CK</i>				0.04	0.74	0.89
<i>YX42B</i>		x		0.07	0.70	0.56
ZD-129	x			0.10	0.67	0.89
ZD41				0.08	0.72	0.91
ZD-47		x		0.07	0.75	0.84
ZD-48				0.06	0.76	0.92
ZD-49		x		0.07	0.65	0.80
ZD50	x	x		0.10	0.85	0.81
ZH-11-94				0.07	0.83	0.80
ZH-1-94				0.04	0.82	0.94

SAMPLE NAME	Excess $^{40}\text{Ar}^*$		Age Max	^{39}f correlated		C_{fig} (raw)
	Low T	High T		Low limit	High limit	
ZH-2B				0.02	0.94	0.90
ZH3KB				0.03	0.91	0.82
ZH-9A-94				0.08	0.86	0.94

ii Low T $^{40}\text{Ar}_E$ extends beyond 10% of initial gas released

ii Initial ^{39}Ar fraction contaminated by $^{40}\text{Ar}_E$

iii ^{39}Ar fraction degassed below melting ($\leq 1100^\circ\text{C}$)

Italicized samples were processed using temperature cycling

Table 2. Difference between Laboratory and MDD correlation

Sample name	LAB C_{fg}	MDD C_{fg}	MDD-LAB C_{fg}	E (kcal/mol)	$\log(D_p/r_o^2)$ (s^{-1})	Sample name	LAB C_{fg}	MDD C_{fg}	MDD-LAB C_{fg}	E (kcal/mol)	$\log(D_p/r_o^2)$ (s^{-1})
487	0.916	0.952	0.035	47.5	6.29	n13	0.988	0.987	-0.001	48.8	6.41
627	0.965	0.967	0.002	39.0	3.54	n14	0.892	0.929	0.037	59.1	9.31
639krx	0.927	0.947	0.020	48.3	4.76	n16	0.851	0.930	0.079	52.9	7.73
93-ng-39	0.985	0.985	0.000	46.2	5.13	n17a	0.877	0.971	0.093	48.4	5.64
940	0.911	0.950	0.039	45.3	5.61	n21	0.904	0.977	0.073	46.0	5.00
96-mx-005	0.975	0.979	0.004	57.2	8.32	n5	0.969	0.984	0.015	50.2	6.16
98-8-21-2a	0.947	0.965	0.018	40.6	3.98	n6	0.954	0.990	0.036	38.9	2.86
98-8-9-5	0.949	0.993	0.044	35.8	3.01	n8	0.955	0.957	0.002	46.8	5.29
98-8-9-6	0.972	0.988	0.016	42.5	4.64	n9	0.952	0.941	-0.011	45.0	5.06
ac	0.910	0.998	0.088	39.5	2.82	ng17	0.921	0.962	0.041	42.2	3.89
cb2493kf	0.961	0.982	0.021	53.8	7.52	ng37	0.955	0.965	0.009	44.9	4.58
cg194	0.950	0.997	0.047	37.3	2.60	ng6	0.910	0.982	0.073	47.2	5.45
ch-30	0.934	0.978	0.044	41.7	4.85	pn794	0.981	0.997	0.016	40.7	3.15
clbb19kf	0.848	0.926	0.078	40.1	4.04	pn-995	0.868	0.987	0.119	42.8	3.87
cm1	0.910	0.997	0.086	52.0	7.12	pp1	0.959	0.991	0.032	47.1	5.08
cp128	0.947	0.992	0.045	53.6	6.54	qh1	0.954	0.961	0.007	48.4	5.25
cv	0.959	0.973	0.014	51.4	5.84	qh-3	0.895	0.918	0.023	59.1	8.94
dc10c	0.883	0.928	0.045	48.0	6.22	sem394kf	0.943	0.985	0.041	46.0	5.00
dc2a	0.924	0.938	0.013	47.0	6.37	sem694kf	0.977	0.983	0.006	63.9	9.50
dl3	0.985	0.986	0.002	45.1	4.01	sfh	0.883	0.946	0.064	39.7	3.38
dsc	0.960	0.970	0.010	65.3	10.15	sj394	0.912	0.989	0.076	39.7	2.26
f185	0.909	0.913	0.005	60.0	8.68	sm11	0.914	0.980	0.066	29.9	0.80
f188	0.892	0.915	0.023	61.4	9.70	sy	0.934	0.998	0.064	43.8	3.88
f223	0.934	0.945	0.010	46.0	5.00	tr210	0.878	0.938	0.060	40.7	4.17
gr04	0.886	0.987	0.101	37.1	3.45	trbb86	0.965	0.989	0.024	47.6	5.65
gr11	0.897	0.903	0.006	63.6	10.25	v103kf	0.870	0.888	0.018	53.9	7.51
gr12	0.938	0.994	0.056	46.7	5.71	v12kf	0.898	0.987	0.088	59.6	9.17
gr13	0.913	0.958	0.045	46.7	5.26	v4kf	0.873	0.981	0.109	56.3	8.14
gr14	0.905	0.961	0.056	45.6	5.07	ya24	0.943	0.968	0.025	49.2	6.13
gr15	0.936	0.953	0.017	49.8	6.26	yan11	0.965	0.983	0.019	59.9	8.98
gr16	0.889	0.971	0.082	50.6	6.16	yans1	0.968	0.955	-0.013	55.6	7.61
gr18	0.934	0.977	0.043	47.5	5.11	yans-6	0.971	0.978	0.008	48.6	5.74
gr19	0.963	0.985	0.022	44.3	4.45	yn27	0.937	0.986	0.050	39.6	3.61
gr20	0.917	0.969	0.053	39.3	3.15	yu38k	0.870	0.971	0.101	45.9	4.34
kail2k	0.904	0.985	0.082	45.1	4.51	yu97k	0.954	0.980	0.026	49.4	5.13
mca994kf	0.959	0.952	-0.007	64.8	10.73	yx41ck	0.883	0.989	0.106	41.7	3.73
mh8914k	0.940	0.947	0.008	47.1	5.26	zd-129	0.902	0.930	0.029	42.1	3.76
mn1	0.935	0.949	0.015	44.2	4.03	zd41	0.915	0.917	0.002	61.0	9.19
mn7	0.901	0.972	0.070	43.5	3.61	zd-48	0.898	0.916	0.018	59.7	8.51
mp17	0.978	0.999	0.020	51.4	5.38	zh-1-94	0.925	0.970	0.045	37.8	2.49
n10	0.962	0.995	0.033	38.9	2.73	zh-2b	0.888	0.906	0.018	49.5	5.31
n11	0.947	0.970	0.023	55.7	7.55	zh-9a-94	0.937	0.950	0.013	43.1	4.89
n12	0.975	0.986	0.011	44.5	5.27						

Table 3: Domain distributions for recrystallization models

Domain #	$\log(D_0/\rho^2)$	Model A		Contributing Domain	Model B		Contributing Domain
		K % distribution (ϕ)			K % distribution (ϕ)		
		Initial	¹ Final		Initial	² Final	
A1	5.877	2.314	11.570	A8	5.785	11.57	A5
A2	5.124	3.235	16.174	A7	8.087	16.174	A6
A3	4.308	2.251	11.256	A6	5.628	11.256	A7
A4	3.153	12.234	24.468	A5	12.234	24.468	A8
A5	2.427	15.052	2.818		8.603	2.818	
A6	1.972	25.254	16.249		24.336	16.249	
A7	0.918	21.157	8.218		13.846	8.218	
A8	0.487	18.503	9.247		21.481	9.247	

¹ Proportion of sample altered = 43.4%

² Proportion of sample altered = 31.7%

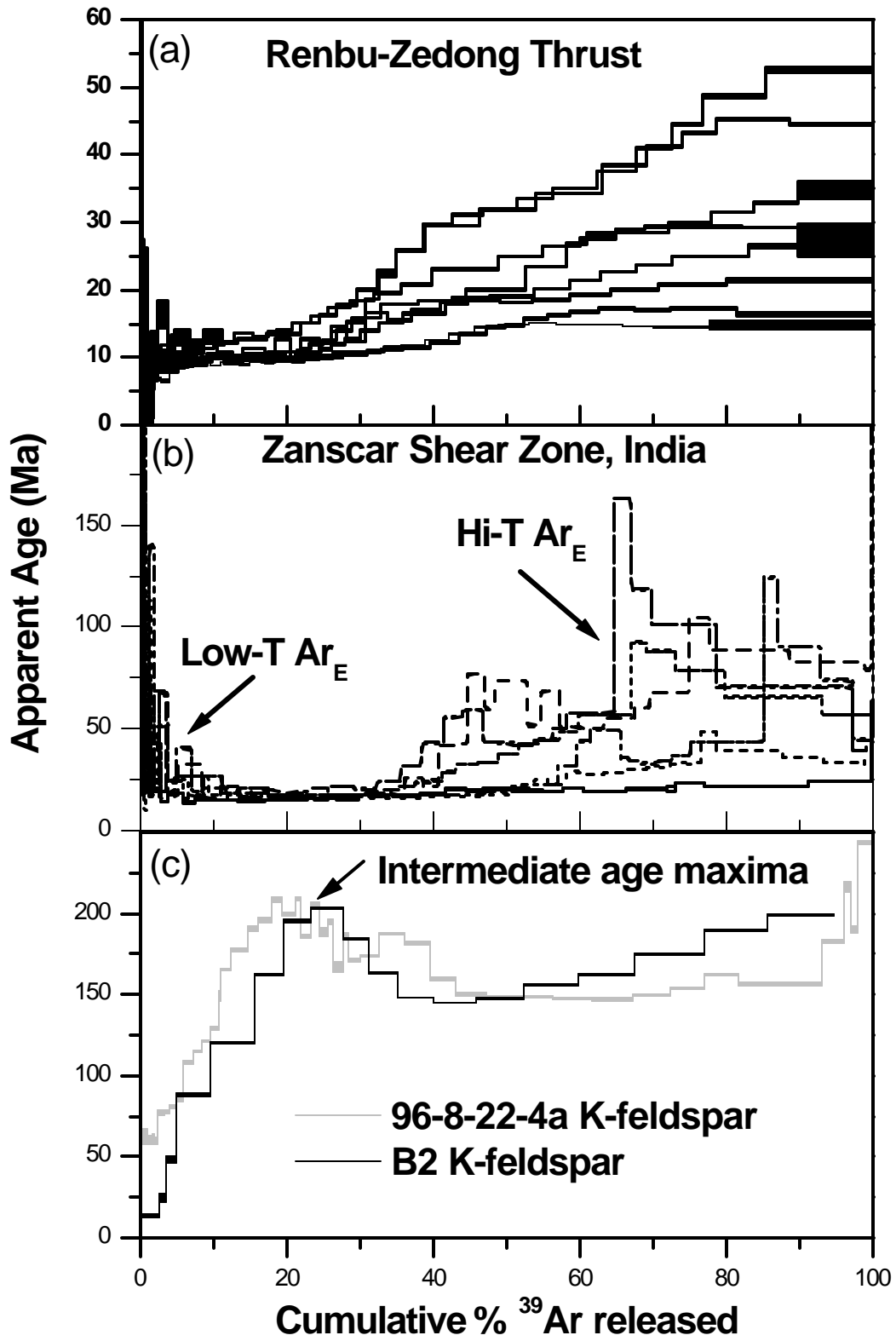


Figure 1 - MS# W0896 - Lovera et. al.

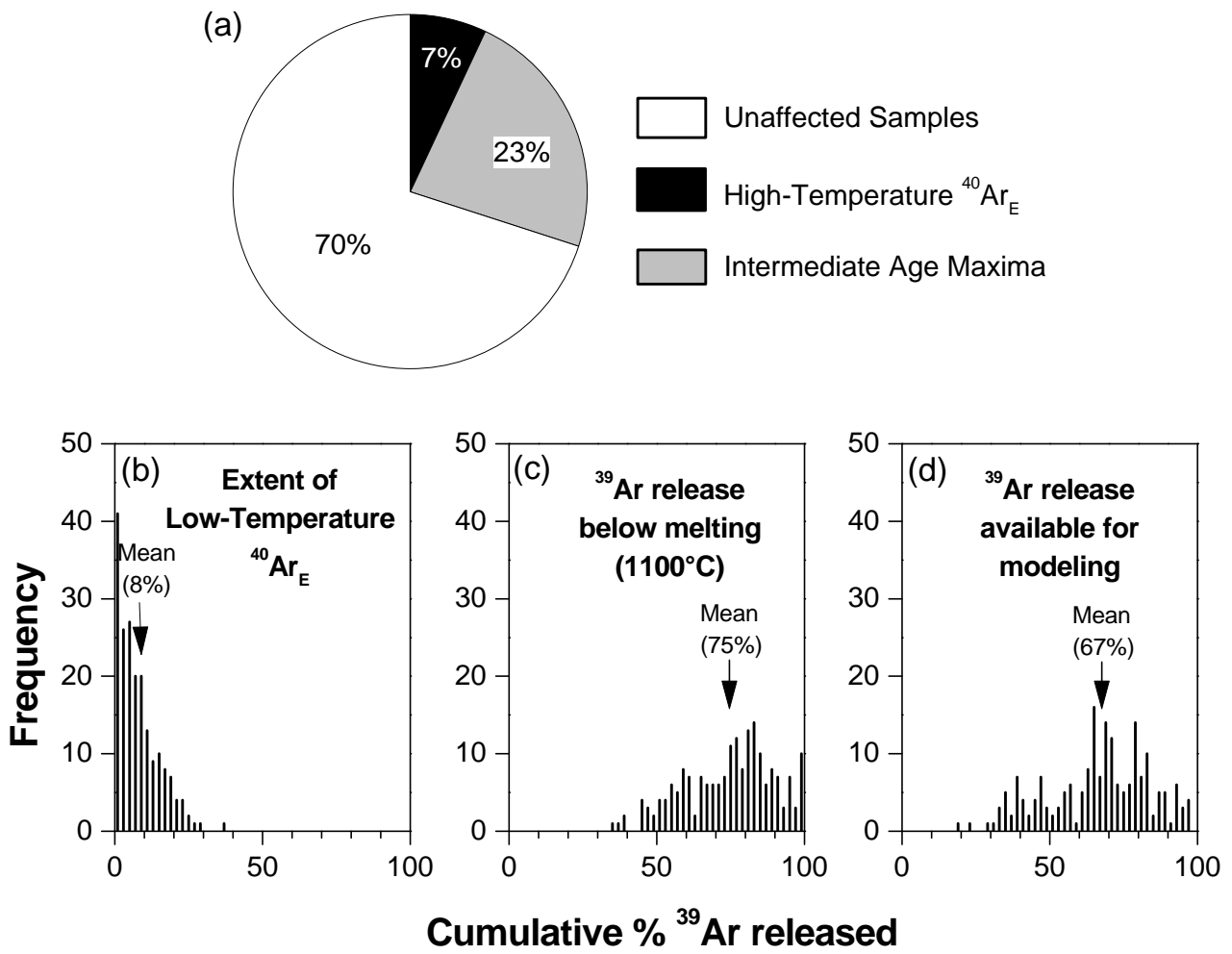


Figure 2

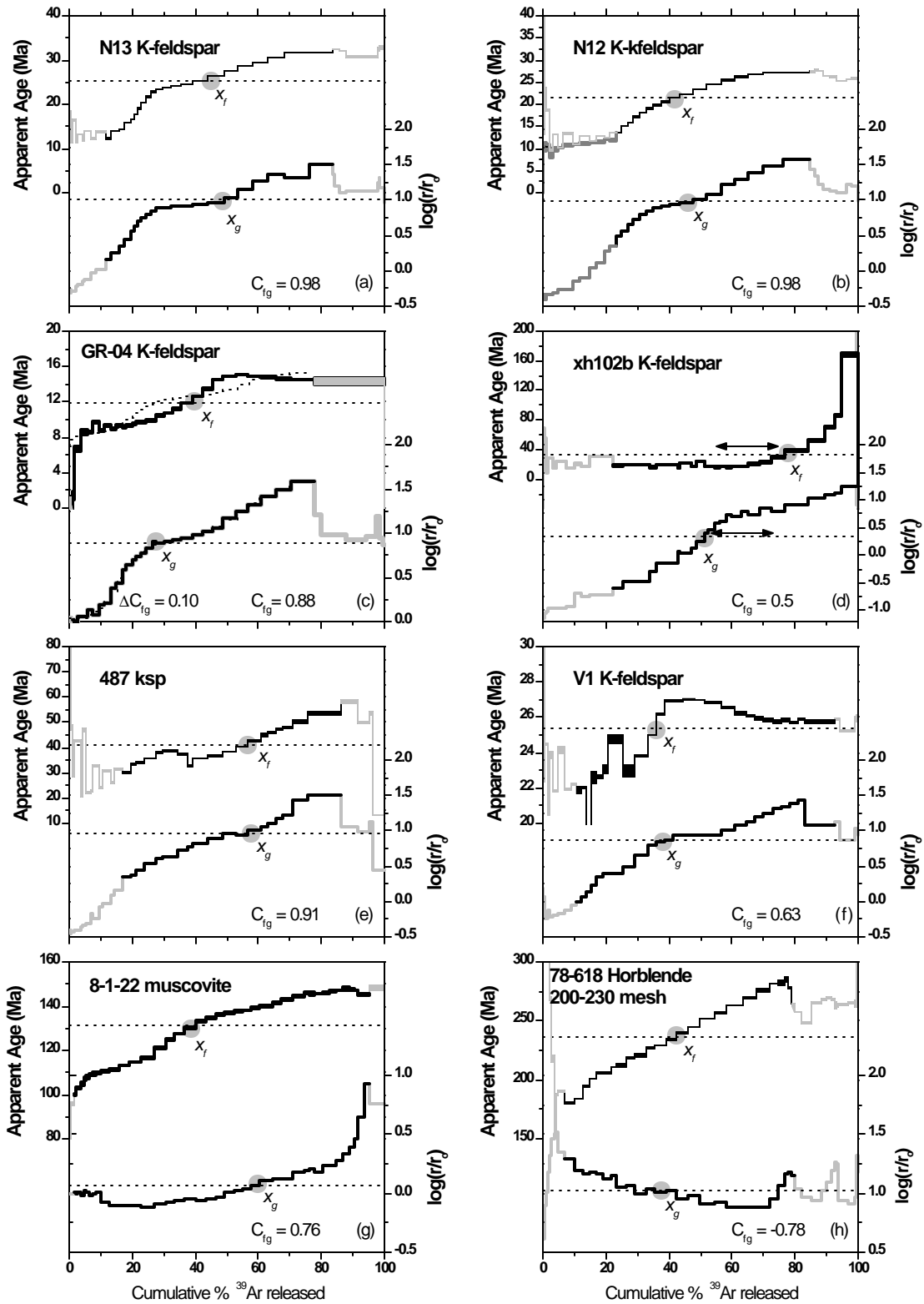


Figure 3 - MS# W0896 - Lovera et. al.

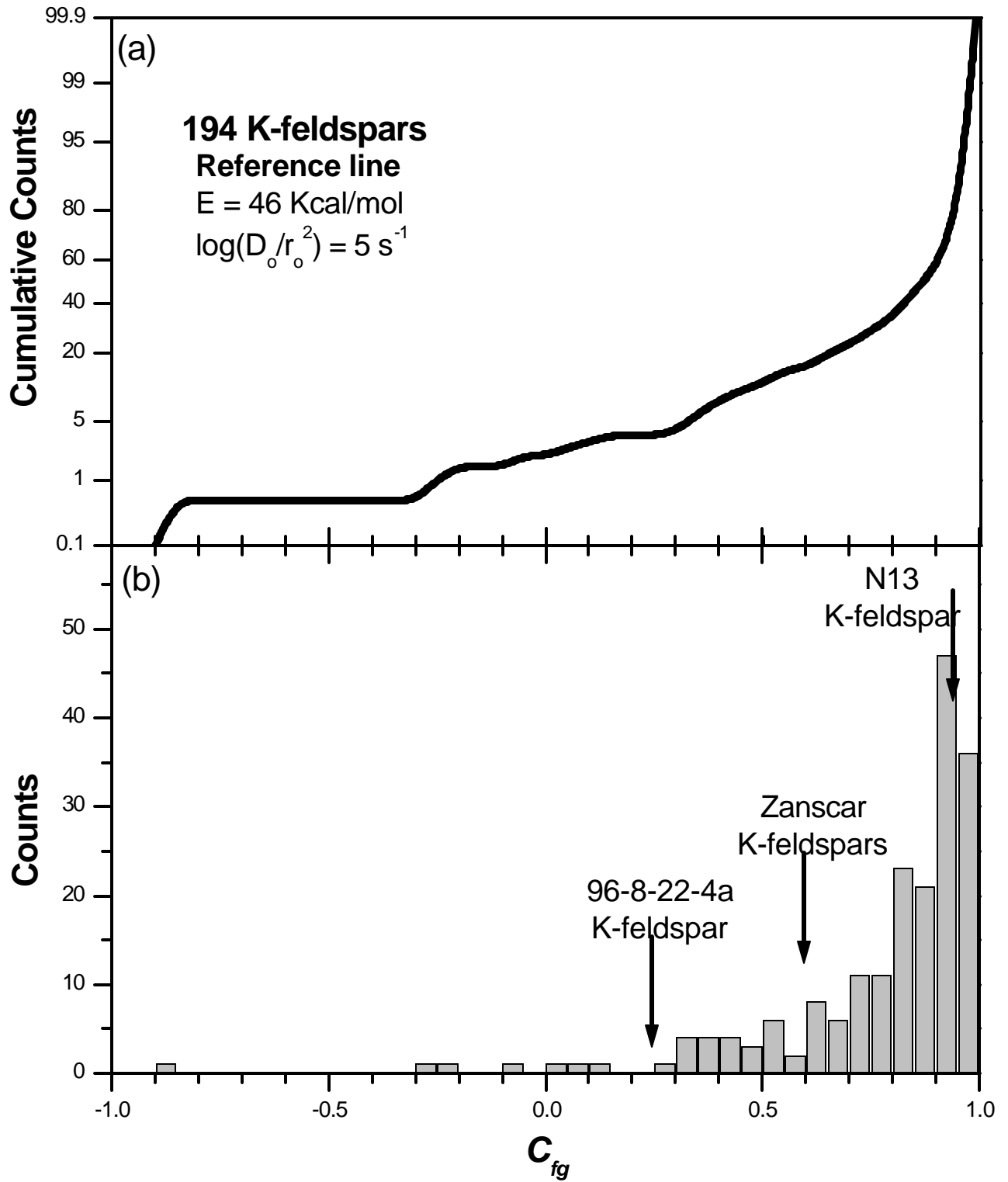


Figure 4- MS# W0896 - Lovera et. al.

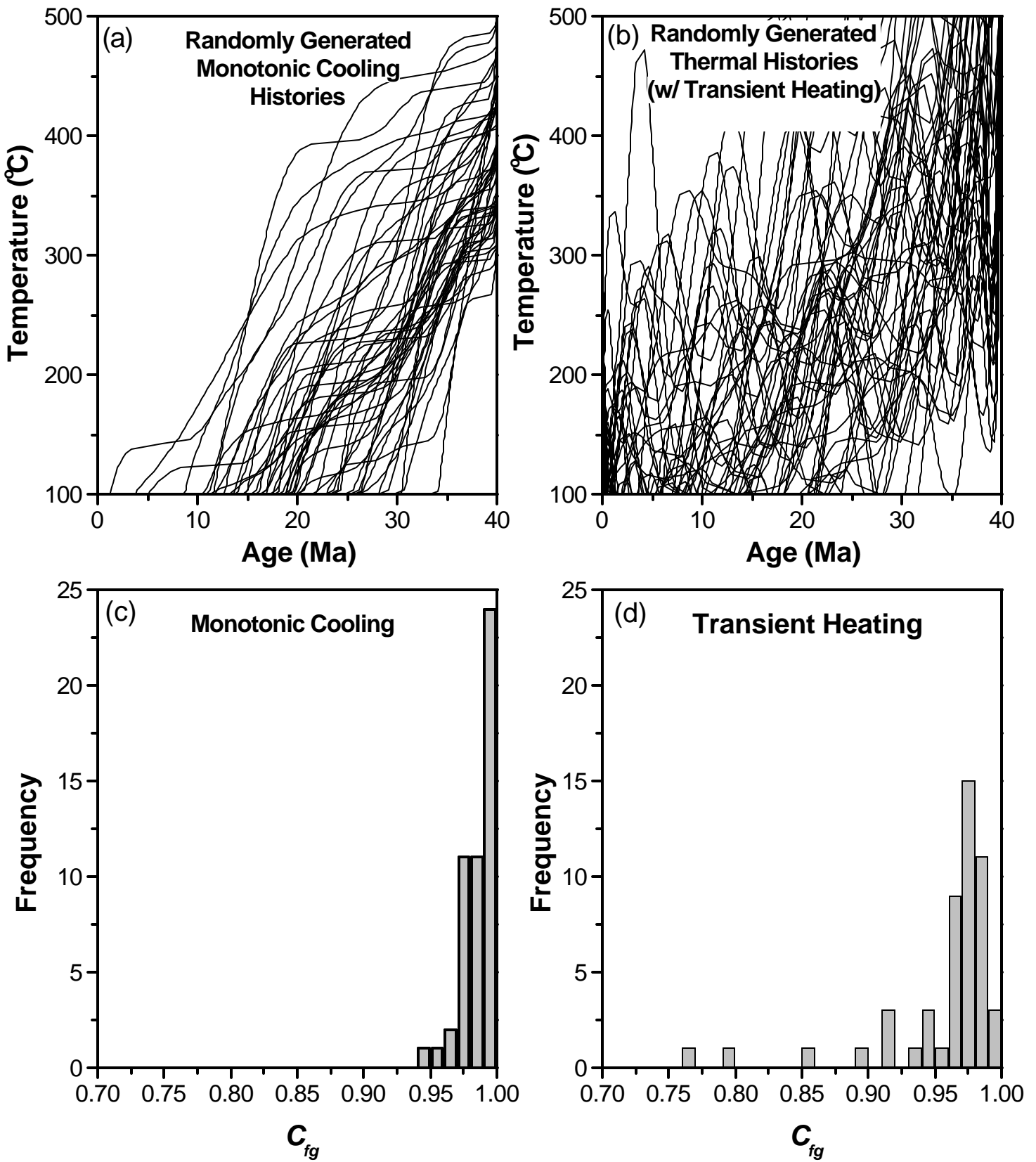


Figure 5 - MS# W0896 - Lovera et. al.

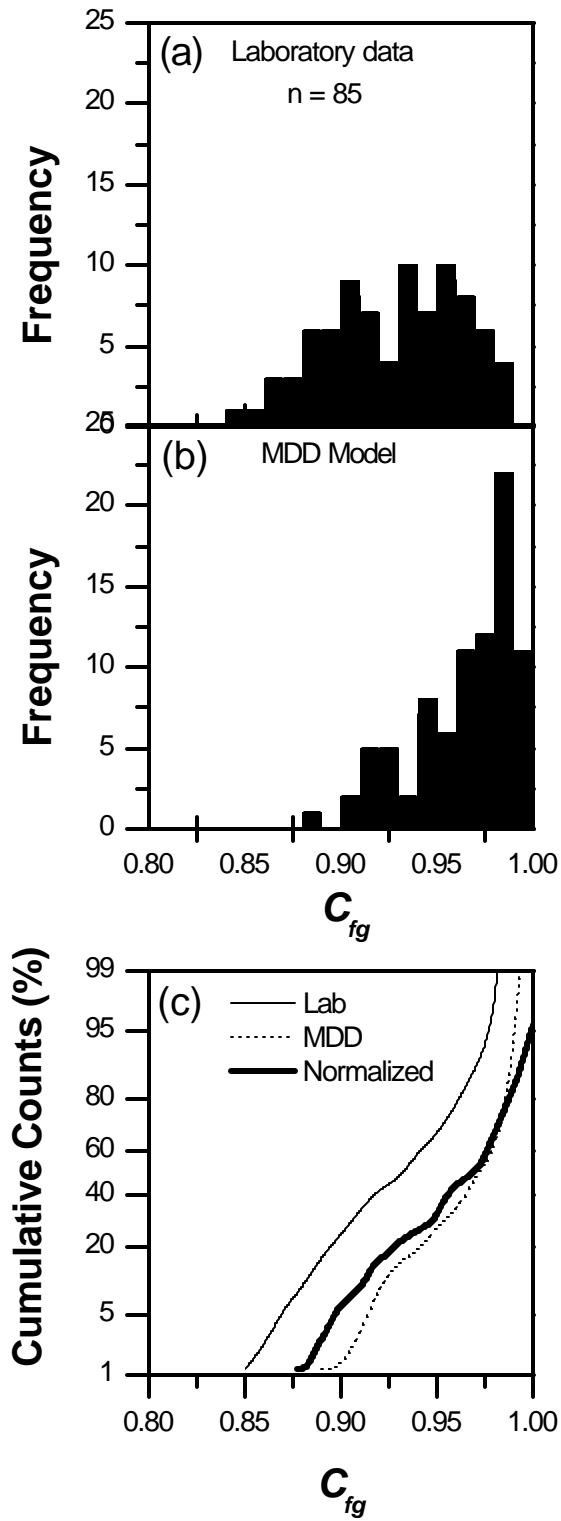


Figure 6 - MS# W0896 - Lovera et. al.

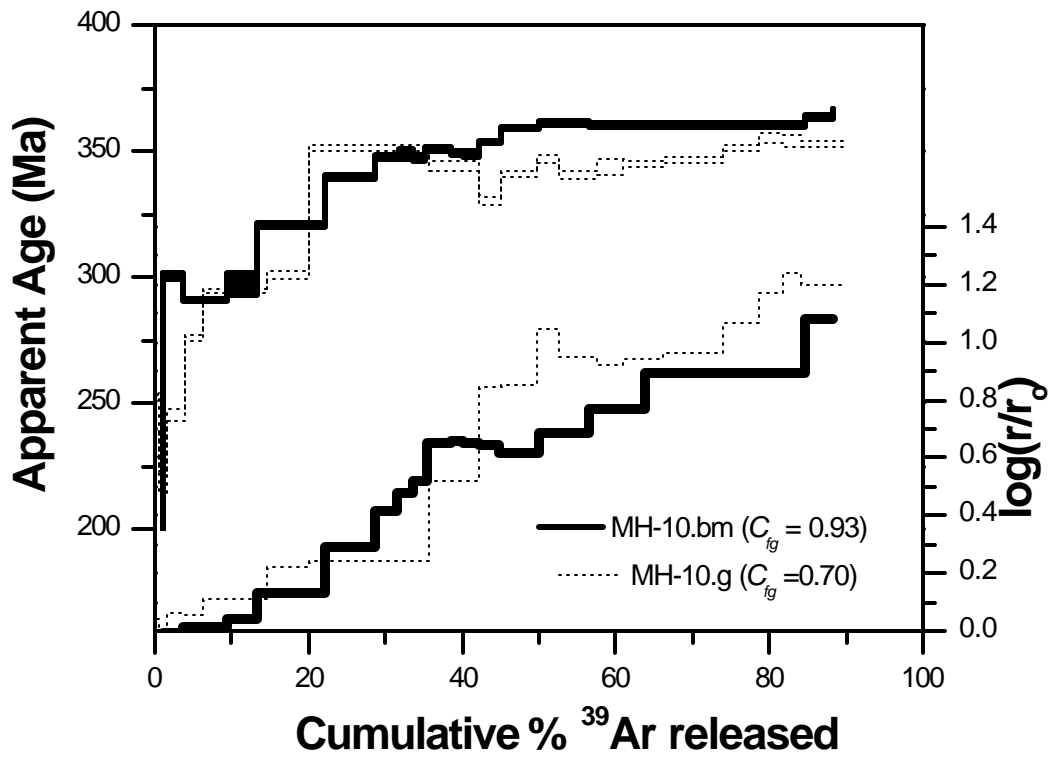


Figure 7 - MS# W0896 - Lovera et. al.

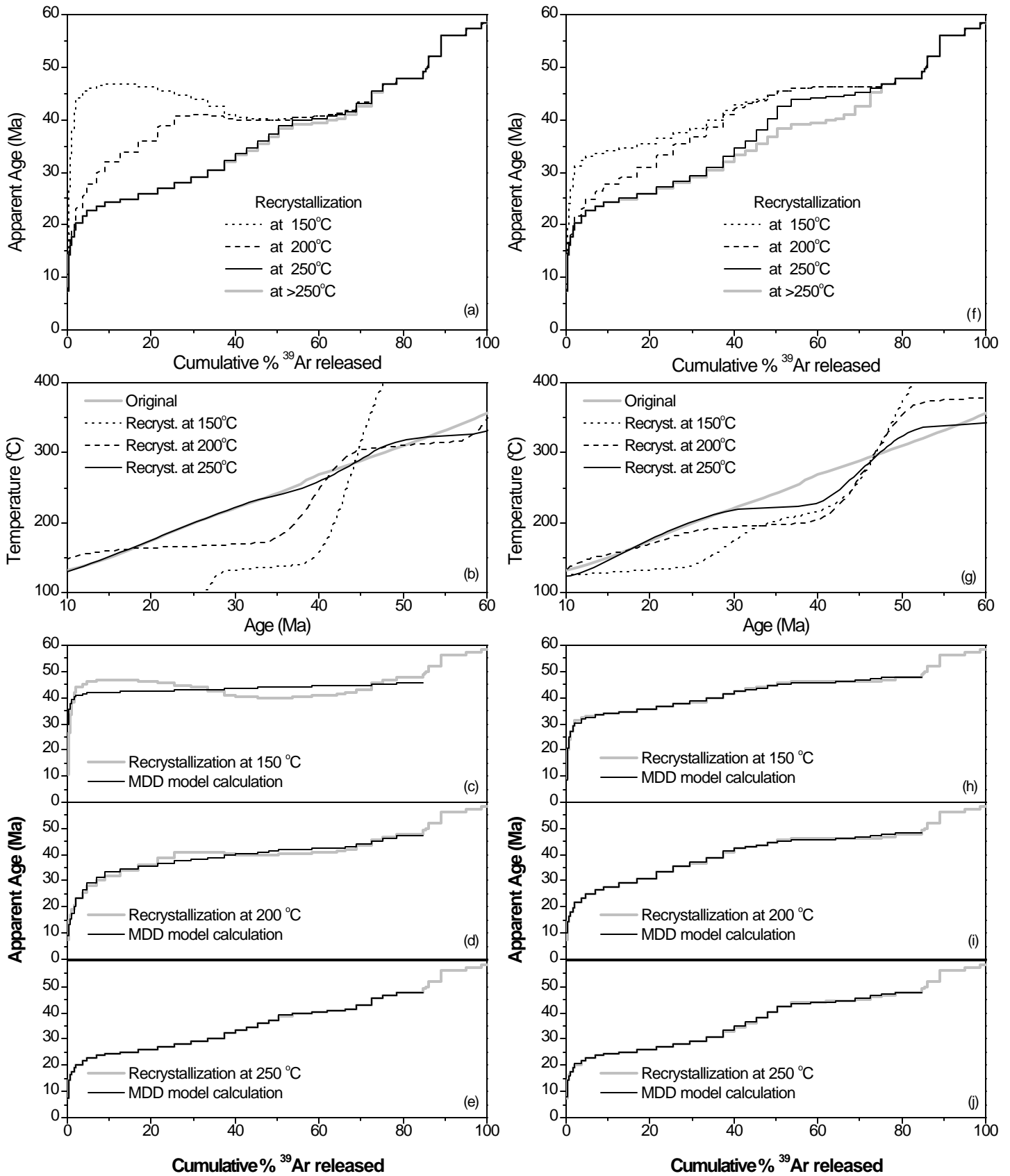


Figure 8 - MS# W0896 - Lovera et. al.

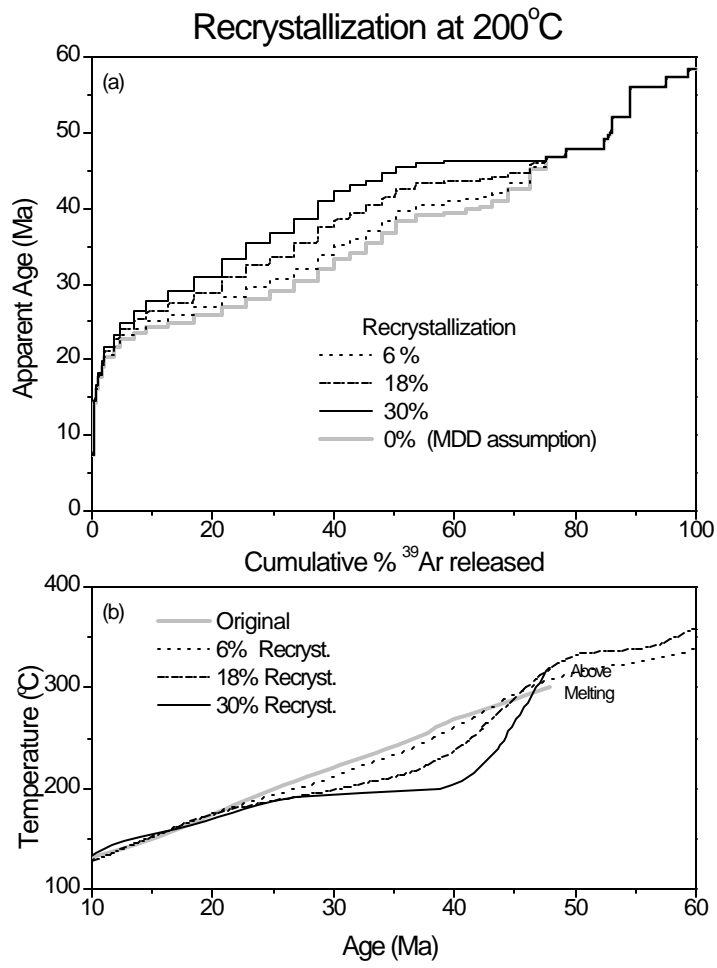


Figure 9 - MS# W0896 - Lovera et. al.

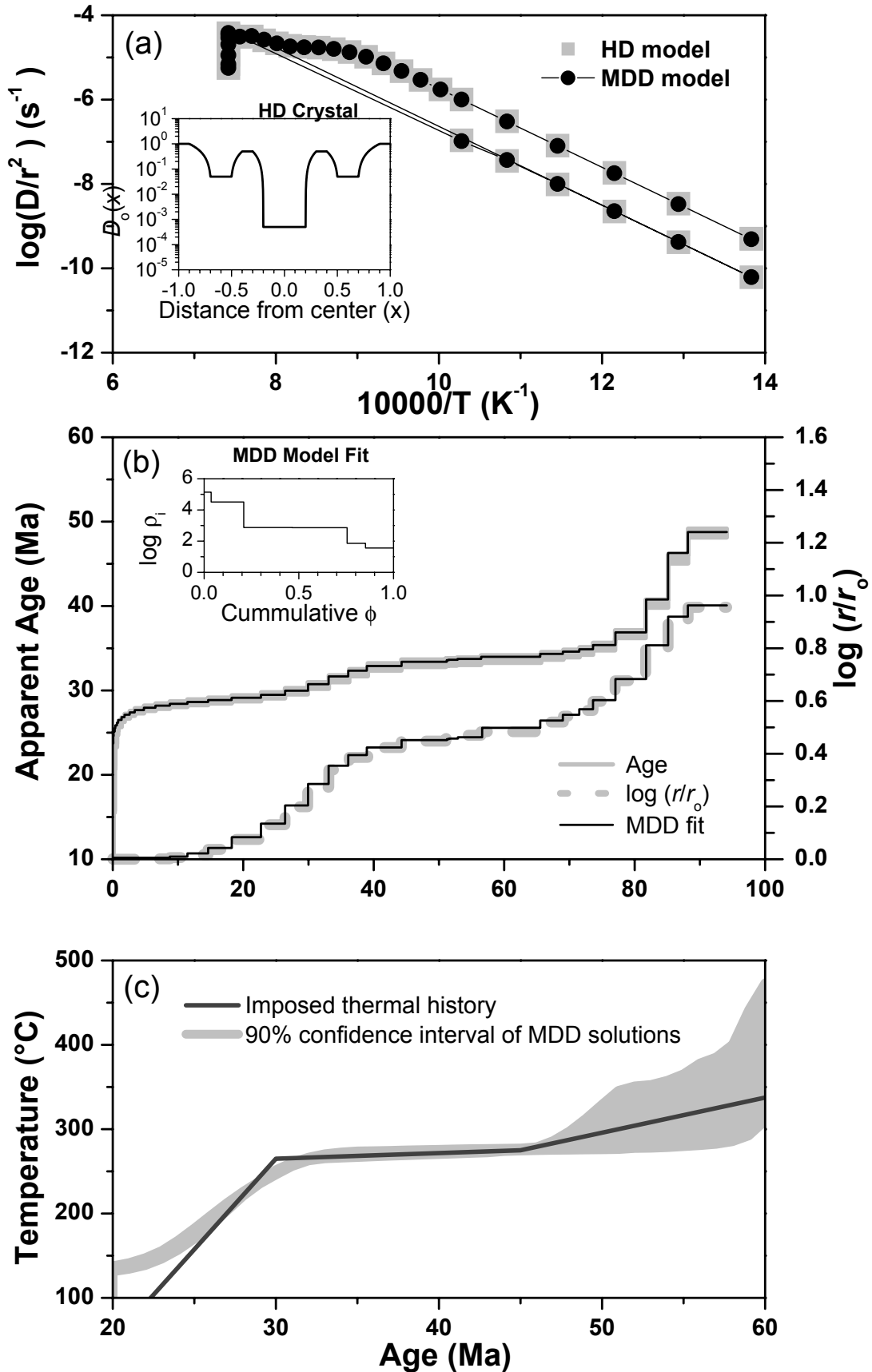


Figure 10 - MS#W0896 - Lovera et al.